Review/Synthèse

Nonlinear acoustic applications for material characterization: A review

Yongping Zheng, Roman Gr. Maev, and Igor Yu. Solodov

Abstract: The nonlinear acoustic applications for material characterization are reviewed. The general theoretical analysis of the effects of nonlinearity, dissipation, dispersion, and diffraction on intense acoustic-wave propagation is given. Acoustic nonlinear parameters and their determination methods are introduced. The investigations of nonlinear acoustic applications for solid material evaluation are discussed for different levels of disruption, from asymmetry of lattice structure and dislocation in crystals to disbonds and cracks in engineering materials. The experimental methods involved in these investigations are also considered. The techniques used for nonlinear acoustic imaging are divided into two categories, concerned with resolution improvement by using higher harmonics, and nonlinear parametric imaging. The nonlinear acoustic applications in biomedical imaging, acoustic microscopy, and nonlinear nondestructive evaluation are presented. Finally, the issues that need further investigations in this area are discussed.

PACS Nos.: 43.25, 62.65, 62.20M

Résumé: Nous examinons l'utilisation de l'acoustique non-linéaire pour la caractérisation des matériaux. Nous présentons la méthode générale d'analyse des effets non-linéaires, de dissipation, de dispersion et de diffraction dans la propagation d'ondes acoustiques de haute intensité. Nous introduisons les paramètres de l'acoustique non-linéaire avec les méthodes pour les déterminer. Nous discutons l'étude des solides via l'acoustique non-linéaire pour différents niveaux de rupture cristalline, de l'asymétrie du réseau et des dislocations jusqu'aux bris de lien et aux fendillements dans les matériaux d'ingénieur. Nous revisons la méthode expérimentale suivie. Les techniques utilisées en imagerie par acoustique non-linéaire se divisent en deux catégories : l'amélioration de la résolution par l'introduction d'harmoniques d'ordre plus élevé et l'imagerie paramétrique non-linéaire. Nous soulignons leur utilisation en imagerie biomédicale, en microscopie acoustique et en NDE non-linéaire. Finalement, nous mentionnons les questions qui exigent une étude plus approfondie.

[Traduit par la rédaction]

Received October 9, 1998. Accepted October 6, 1999.

Y. Zheng and R.Gr. Maev.[1] Ultrasonic Research Laboratory, Department of Physics, University of Windsor, Windsor, ON N9B 3P4, Canada.
I.Yu. Solodov. Department of Physics, Moscow State University, Moscow 119899, Russia.

[1] Corresponding author: **Telephone:** : (519) 253-4232 ext. 2661; **FAX:** : (519) 973-7075; **e-mail:** : maev@uwindsor.ca

1. Introduction

The interaction of an acoustic signal with matter is said to be "linear," if the response of the material and the strength of the output signal vary linearly with the strength of the input signal, as in Hooke's law. The majority of well-known acoustic phenomena are associated with linear elastic material properties. However, for high input signal strengths, or for materials with some special properties, a family of new "nonlinear effects" appear such as acoustic-wave-form distortion due to amplitude-dependent wave propagation velocity, higher harmonics generation, or acoustic rectification of the input signal, sum and difference frequency generation for multiple input signals, acoustic streaming, self-focusing, etc. Some of these effects have close analogs in optics [1] and other branches of physics, and they are increasingly used for nondestructive characterization of materials and damage detection in industrial products.

Problems of nonlinear acoustics have been studied since the 18th century [2]. A number of early papers were compiled by Beyer [3] in a collection of benchmark papers on nonlinear acoustics. From the 1960s to the 1970s, underwater applications of nonlinear acoustics, concentrating around the parametric array problem, were investigated in detail [4–6]. By the early 1970s, parametric arrays were used for both civilian and military applications, and numerous investigations were carried out in this field [7]. Considerable theoretical progress in understanding nonlinear acoustic phenomena was also accomplished during that period [8–14]. Most recently, a book edited by Blackstock and Hamilton [2] provided reviews on the theory and some applications of nonlinear acoustics. However, a comprehensive review on nonlinear acoustic applications for material characterization is still lacking in the literature.

During the last few decades, various aspects of nonlinear acoustics have been investigated in many different fields pertaining to material characterization. These fields cover condensed matter physics, acousto-optics, low-temperature research, Earth studies, chemical physics, biophysics, biomedical engineering, nondestructive testing, and acoustic microscopy. In condensed matter physics, nonlinear acoustic techniques have been used for many years to determine the high-order elastic constants of various solids and their temperature dependence, and to investigate lattice structure and dislocations in crystals [15,16]. In acousto-optics, various schemes of nonlinear interaction between acoustic waves and optical beams have been investigated and used to determine nonlinear parameters of the medium [17,18]. In addition, optical methods using laser interferometers have been successfully applied for the detection of nonlinear acoustic vibrations in the materials [19]. In low-temperature research, nonlinear acoustical investigations of various media, such as liquid helium, copper, and some high-temperature superconductors have been performed. Nonlinear coefficients were found to be much more sensitive to temperature variations than linear parameters [20]. In Earth studies, nonlinear acoustics have been used to investigate the elastic nonlinear effects in grained materials and rocks [21,22] concerning their prospective applications in geology and seismology [23,24]. In chemical physics, the nonlinear parameters of various pure and mixed liquids have been determined. Their dependence on molecular properties, concentration of liquids, and chemical reaction process has also been widely investigated [25]. In biophysics, an increasingly important parameter for characterizing body tissues is the acoustic nonlinearity of the specimen. Nonlinear properties of various biological media at the tissue level, such as liver, and at the molecular level, such as amino acids and proteins, have been investigated [25]. The effects of nonlinear propagation of acoustic waves have been widely used in lithotripsy and acoustic physiotherapy of soft tissues [26]. Meanwhile, in biomedical engineering, many investigations have been conducted for the improvement of the resolution in diagnostic medical ultrasound equipment by using nonlinear propagation and reflection of ultrasound [27]. The quantitative imaging of the nonlinear parameter of soft tissues has also been attempted [28].

Besides various applications of nonlinear acoustics described above, one of its most exciting potentials is believed to be the application in nondestructive testing. An important reason for this prospect is that high nonlinear properties are always closely related to the number and specific nature of defects in materials [29]. Since the last decade, a great deal of interest has been shown in the nonlinear acoustic nondestructive evaluation of various defects in materials of practical importance. Nonlinear acoustic

techniques have been proven to be useful for the measurements of adhesion strength in layered structures [30], nondestructive detection of fractured defects in crystals [31], ceramics [32], carbon electrodes [33], and concrete structures [34], as well as fatigue cracks in metals, such as steels, titanium, and aluminum alloys [35]. The acoustic frequency employed ranged from several hundred Hz for standing wave detection of problems with space shuttle ceramic tiles [32] to over 15 GHz for an acoustic microscope operating with pressurized super-fluid helium [36]. Some defects in materials, such as internal stresses, microfatigue cracks, and zero-volume disbonds are usually the forerunners of the main cracking and subsequent failure of the material. However, conventional linear acoustic characteristics, such as sound velocity, attenuation, transmission, and reflection factors are found to be insensitive to these inhomogeneities of materials. Nonlinear acoustic methods for the detection of these kinds of defects in materials have been recently proposed in the literature [31,37].

On the other hand, nonlinear acoustics has also been used in acoustic microscopy since the first experiments by Kompfner and Lemons [38]. Besides the improvement in resolution by using higher harmonic signals [39], some other effects, such as quantitative imaging of material properties have been observed with the acoustic microscope operating in nonlinear mode [40].

The purpose of this review is to highlight the applications of nonlinear acoustics in material characterizations that have been developed over the last decades. The review begins with an introduction to the theoretical foundations of nonlinear acoustics. Basic nonlinear equations for intense acoustic-wave propagation in various media are formulated and used to introduce acoustic nonlinearity parameters for various media. The effects of nonlinearity, dissipation, dispersion, and diffraction on nonlinear acoustic-wave propagation are analyzed. Some remarks on the nonlinear properties of "nonclassical" materials conclude general theoretical considerations. In Sects. 3 and 4, the investigations of nonlinear acoustic applications for solid material evaluation are highlighted. Nonlinear acoustic methods for the characterization of solid materials with different levels of disruption such as lattice structure, dislocations, alloying, disbonds, and cracks are introduced. After a review of nonlinear acoustic experimental techniques, nonlinear acoustic imaging is considered. The investigations of nonlinear acoustic imaging are introduced for both improvement of image resolution and nonlinear parametric imaging. Finally, nonlinear acoustic applications for material characterization are summarized and some subjects for further investigations in this area are proposed.

2. Theoretical considerations

In the linear theory of acoustic-wave propagation, sound wave velocity in a medium is considered to be a constant. Thus, a monochromatic acoustic wave never distorts during its propagation in a medium, although its amplitude is reduced due to dissipation and diffraction. Accordingly, two elastic waves do not interact with each other in the linear theory (superposition principle). Linear theory is based on the assumption that neither the density nor the elasticity of a medium depends on the wave amplitude. Such an approach is sensible only if the changes in strain, pressure, temperature, and density caused by an acoustic wave are negligible. As the wave amplitude increases, amplitude-dependent (nonlinear) effects are manifested in the equations of state and continuity of the medium, resulting in nonlinear equations of motion. At low dissipation and weak dispersion, even relatively small-amplitude nonlinear effects can be accumulated during a sound wave propagation and give rise to a substantial nonlinear distortion of an acoustic wave, efficient interaction between elastic waves, and other peculiar nonlinear phenomena.

2.1. Nonlinear material coefficients

The acoustic nonlinearity of a material can be generally introduced by using the expression for the propagation speed of a forward traveling plane wave of finite amplitude [8,41]:

$$V = c_0(1 + \beta_2 M) \tag{1}$$

where c_0 is the velocity of sound for a wave of infinitesimal amplitude, $M = u/c_0$ is the acoustic Mach number, u is the particle velocity, and β_2 is the coefficient of the second-order acoustic nonlinearity. Equation (1) shows that each point of the particle velocity wave form propagates at a speed determined by its local value of u for a finite-amplitude acoustic signal. As a result, the wave distorts during propagation at a rate determined by β_2. For $\beta_2 > 0$, the peaks of a particle velocity profile travel faster than the troughs, therefore, initially, the harmonic acoustic-wave form distorts after it has propagated for some distance in a nonlinear material being transformed into a saw-tooth-like velocity wave. With thermal and viscous losses taken into account, such a process can eventually lead to a shock formation. In the frequency domain, the distortion of the wave form causes the generation of higher harmonics. This means that nonlinearity results in an acoustic energy transfer from the fundamental frequency to higher harmonics, which is one of the fundamental principles for nonlinear acoustic material characterization. In addition, a nonlinear interaction can be expected between two acoustic waves passing through each other in a nonlinear medium.

The acoustic nonlinear coefficient β_2, representing the rate of acoustic-wave distortion and the degree of interaction of two acoustic waves, is thus an important parameter that can be used to characterize acoustic nonlinear properties of gases, liquids, and solids. Nonlinear elastic behavior of any of these media is due to nonlinear contributions from the relations describing the adiabatic oscillations (the equation of state) and continuity of the medium into equations of motion. As a result, for a one-dimensional acoustic wave propagating along the x-axis in gases and liquids one obtains a nonlinear equation of motion in Lagrangian coordinates [42]:

$$\frac{\partial^2 U}{\partial t^2} = \left(\frac{\rho}{\rho_0}\right)^2 \left(\frac{\partial p}{\partial \rho}\right)_s \frac{\partial^2 U}{\partial x^2} \tag{2}$$

where U is the particle displacement, ρ_0 and ρ are, correspondingly, the static and dynamic densities, p is the pressure, and s is the entropy. Two factors in the right-hand side of (2) illustrate the two sources of the nonlinearity mentioned above. Substituting the continuity relation $\rho_0 = \rho(1 + \partial U/\partial x)$, the adiabatic equation of state $p = p_0(\rho/\rho_0)^\gamma$, and after retaining the quadratic terms in $\partial U/\partial x$, (2) takes an explicit nonlinear form with an amplitude-dependent wave velocity:

$$\frac{\partial^2 U}{\partial t^2} = c_0^2 \left[1 - (\gamma + 1)\frac{\partial U}{\partial x} + \ldots\right] \frac{\partial^2 U}{\partial x^2} \tag{3}$$

where γ is the ratio of specific heats for gases ($\gamma \cong 1 - 1.67$), and is the experimentally determined parameter for liquids ($\gamma \cong 4 - 12$).

Introducing the acoustic Mach number $M = u/c_0 = -\partial U/\partial x$ into (3) and keeping only these first two terms in the square brackets (because $\partial U/\partial x \ll 1$) after expansion in series one easily obtains formulae (1), where

$$\beta_2 = \frac{\gamma+1}{2} \tag{4}$$

Thus, the nonlinearity coefficient β_2 ranges from 1 to $\cong$1.4 for gases, and varies from $\cong$2.5 to $\cong$6.5 for liquids.

Another way to express β_2 for liquids uses Taylor-series expansion of the pressure–density relation [11,43]:

$$p = p_0 + A\left(\frac{\rho - \rho_0}{\rho_0}\right) + \frac{B}{2}\left(\frac{\rho - \rho_0}{\rho_0}\right)^2 + \ldots \tag{5}$$

Differentiating (5) we obtain:

$$\left[\left(\frac{\partial p}{\partial \rho}\right)_s\right]^{1/2} \cong c_0 \left[1 + \frac{B}{2A}\frac{\rho - \rho_0}{\rho_0}\right] = c_0 \left[1 + \frac{B}{2A}M\right] \tag{6}$$

Combining (6) with a nonlinear contribution from the continuity equation $\rho/\rho_0 = (1 + \partial U/\partial x)^{-1} \approx (1+M)$, from (2) we obtain

$$V = c_0\left[1 + \left(1+\frac{B}{2A}\right)M\right] \tag{7}$$

Equation (7) illustrates the (B/A) contribution in the wave-form distortion determined by $\beta_2 = 1 + \frac{B}{2A}M$. The ratio (B/A) is often used as an alternative to the β_2 nonlinear parameter for liquids.

For acoustic waves in solids, the equation of state is a series expansion of the stress-strain relation, which in a quadratic approximation for the longitudinal wave in an isotropic material turns the equation of motion (2) into an analogous form [42]:

$$\frac{\partial^2 U}{\partial t^2} = c_0^2\left[1 + \frac{C^{\mathrm{III}}}{C^{\mathrm{II}}}\frac{\partial U}{\partial x} + ...\right]\frac{\partial^2 U}{\partial x^2} \tag{8}$$

where C^{II} is a linear combination of the second-order elastic constants $\rho_0 c_0^2 = C^{\mathrm{II}}$, while C^{III} includes the second- and third-order constants.

Similar to the above, from (8) we obtain for the nonlinear coefficient in solids

$$\beta_2 = -\frac{C^{\mathrm{III}}}{2C^{\mathrm{II}}} \tag{9}$$

Thus, depending on the sign of C^{III} nonlinear distortion of longitudinal waves in solids can result in the saw-tooth-like velocity wave form (if $C^{\mathrm{III}} < 0$), or an N-type wave (for $C^{\mathrm{III}} > 0$). The majority of solids possess $C^{\mathrm{III}} < 0$ and hence, $\beta_2 > 0$, however, for some materials like glass or fused silica $\beta_2 < 0$ [8].

If one retains higher than second-order terms in the equation of state for solids (stress–strain expansion), expression (9) can be easily generalized for the nth-order nonlinear coefficient

$$\beta_n = -\frac{C^{n+1}}{n!C^{\mathrm{II}}} \tag{10}$$

Note, that (9) and (10) actually illustrate the definition of β_n as a negative-normalized coefficient of the nth-order term in the equation of state. In another approach [42], using the corresponding coefficients on the right-hand side of (8) and results in values of β_n that are twice as big.

Classical nonlinear acoustics is generally concerned with $n = 2$, since higher harmonics observed in flawless solid materials are usually negligible. In imperfect materials, some specific mechanisms of elastic nonlinearity are involved (Sects. 3.2–3.4) and higher order coefficients should be taken into account.

Introducing the cubic terms in (8), the wave velocity becomes

$$V = c_0\left(1 + \beta_2 M + \left(\frac{3}{2}\right)\beta_3 M^2\right) \tag{11}$$

Formulae (11) shows that the third-order nonlinearity leads to a change in the average value of wave velocity.

To quantify the effect of β_n on the wave distortion we write the expression for the particle velocity wave form corresponding to the velocity variation (1) and a monochromatic driving source of amplitude u_0

$$u(x,t) = u_0 \sin\omega\left[t - \frac{x}{c_0(1+\beta_2 M)}\right] \cong u_0 \sin[\omega t - kx(1 - \beta_2 M)] \tag{12}$$

In the latter formulae, obtained by the first-order series expansion on the Mach number, $k = \omega/c_0$.

According to (12), at $x \cong 0$: $u(x,t) \cong u_0 \sin(\omega t - kx)$, as x increases, the particle velocity profile becomes steeper with a maximum slope at $u = 0$. Calculating the derivative

$$\left(\frac{\partial u}{\partial x}\right)_{u=0} = -\frac{u_0 k(1-\beta_2 M)}{1-u_0(k\beta_2 x/c_0)} \tag{13}$$

one can easily see that $\partial u/\partial x$ becomes negatively infinite, corresponding to a shock wave formed at the so-called discontinuity distance x_D:

$$x_D = (k\beta_2 M_0)^{-1} \tag{14}$$

where $M_0 = u_0/c_0$ is the amplitude Mach number.

For a 1 MHz acoustic wave in water possessing $M_0 \cong 5 \times 10^{-4}$ ($p = p_0 = 10$ atm), one obtains from (14) $x_D \cong 15$ cm [11]. For an arbitrary driving signal $\Phi(t)$, nonlinear wave-form distortion similar to (12) can be written in a more general form

$$u(x,t) \cong \Phi\left[t - \frac{x}{c_0}(1-\beta_2 M)\right] \equiv \Phi\left(\tau + \frac{\beta_2}{c_0^2} u x\right) \quad \text{where} \quad \tau = t - \frac{x}{c_0} \tag{15}$$

By direct substitution one can easily see that (15) is a solution of the so-called simple-wave nonlinear equation

$$\frac{\partial u}{\partial x} - \frac{\beta_2}{c_0^2} u \frac{\partial u}{\partial \tau} = 0 \tag{16}$$

Equation (16) is an alternative form of the second-order nonlinear approximation of (3) and (8). Within this approximation is a full description of the one-dimensional nonlinear wave-form evolution in a nondissipative medium.

The harmonic content of the distorted wave form can be obtained by expanding (12) into a power series of u_0. The second-order expansion, after some transformations based on the assumptions $u_0 =$ const. and $M \ll 1$, yields [44]

$$u(x,t) = u_0 \sin(\omega t - kx) + \frac{\beta_2}{2} \omega M_0^2 x \sin\left[2(\omega t - kx)\right] \tag{17}$$

According to (17), at some distance from a monochromatic source in a nonlinear medium the second harmonic is formed, its amplitude in the fixed-field approximation ($u_0 =$ const.) grows linearly with distance and sound intensity. For large x, the fixed-field approximation breaks due to energy transfer to the second (and higher) harmonics; the nth harmonic amplitude variation with distance becomes proportional to the normalized Bessel function $J_n(nx/x_d)/(nx/x_d)$ and is known as the Fubini–Ghiron solution [11].

In solids, the particle displacement form of (17) is used more frequently. A simple integration of (17) with respect to time shows that the fundamental wave $J_n(nx/x_d)/(nx/x_d)$ will be accompanied by the second-harmonic displacement

$$U_{2\omega} = -\frac{\beta_2}{4} k^2 U_0^2 x \cos[2(\omega t - kx)] \tag{18}$$

Similar analysis in a cubic approximation results in the following expressions for the third-harmonic amplitude:

$$U_{3\omega}^0 = \frac{\beta_2^2}{8} k^4 U_0^3 x^2 \quad \text{for} \quad \frac{\beta_3}{\beta_2} \ll kx \tag{19}$$

$$U_{3\omega}^0 = \frac{\beta_2^2}{8} k^3 U_0^4 x^2 \qquad \text{for} \qquad \frac{\beta_3}{\beta_2} \gg kx \tag{20}$$

Since for ultrasonic frequencies $kx \cong 10^2 - 10^3$, quadratic nonlinearity dominates in "classical" solids where normally $\beta_3/\beta_2^2 \approx 1$ [45], (19) holds. An excessively high level of the third harmonic (observed, for example, for imperfect ("nonclassical") materials) indicates cubic nonlinearity domination in a solid. In this case, (20) is used to determine β_3 and obtain the information on the material fourth-order moduli.

2.2. Methodology for determination of nonlinear parameters

Relations (17)–(20) represent the basis for β_2 and β_3 determination by measuring the amplitudes of the second and third harmonics, this is referred to as the finite-amplitude (or spectral) method. It uses the fact that the β_2 and β_3 values are proportional to the slope of the corresponding harmonic growth with distance and can be determined by measuring harmonic amplitudes $U_{2\omega}^0$ and $U_{3\omega}^0$ for a given distance and fundamental wave parameters. For example, using amplitude measurements of the second-harmonic amplitude in solids from (18) we obtain

$$|\beta_2| = \frac{4U_{2\omega}^0}{k^2 x U_0^2} \tag{21}$$

This relation allows us to obtain the $|\beta_2|$ value; the sign of the nonlinear parameter can be determined from the phase analysis of the ω- and 2ω-waves. In solids, the expression for C^{III} in (9) can be frequently broken down into [46]

$$C^{\mathrm{III}} = 3C^{\mathrm{II}} + c^{\mathrm{III}} \tag{22}$$

where C^{III} is the combination of the third-order elastic constants only. Therefore, by determining (according (21)) the nonlinearity coefficient for solids (often denoted as Γ and called the nonlinear parameter) one can calculate the third-order elastic constants c^{III} from the following expression derived from (9) and (22):

$$\beta_2 \equiv \Gamma = -\left(\frac{3}{2} + \frac{c^{\mathrm{III}}}{2C^{\mathrm{II}}}\right) \tag{23}$$

Similarly to the above, from (17) we can obtain β_2 in terms of acoustic pressure $p = \rho_0 c_0 u$, which is easier to measure in liquids (and gases),

$$\beta_2 = \frac{2\rho_0 c_0^3 p_{2\omega}}{\omega x p_\omega^2} \tag{24}$$

More often, however, the B/A parameter is used for characterization of liquids and biological media; it can be determined by measuring the dependence of the sound speed on temperature and pressure, which is referred to as the thermodynamic method and based on the following relations [11]:

$$\frac{B}{A} = 2\rho_0 c_0 \left(\frac{\partial c}{\partial p}\right)_{s,\rho=\rho_0} \equiv 2\rho_0 c_0 \left(\frac{\partial c}{\partial p}\right)_T + \frac{2c_0 T\mu}{C_p}\left(\frac{\partial c}{\partial T}\right)_p \tag{25}$$

where T is the absolute temperature, μ is the volume coefficient of thermal expansion, and C_p the specific heat at constant pressure.

The first term on the right-hand side of (25) is interpreted as the relative increase in sound velocity caused by pressure changes, while the second is brought about by temperature variations. Thus, B/A

can be determined experimentally by measuring the change of the sound speed under the control of the thermodynamic parameters.

Meanwhile, an approach similar to the thermodynamic method has been employed for the study of solid media [47, 48]. An acoustoelastic constant was defined for the characterization of microstructures of solid media [48]:

$$H = \frac{1}{c}\frac{\partial c}{\partial p} \tag{26}$$

This definition is similar to that of B/A in (25), although it is derived in a different way. The acoustoelastic constant H is a material parameter and depends on the second- and third-order elastic constants of the solid media. For anisotropic materials, it also depends on the wave propagation direction and its polarization. It has been used for microstructure evaluation of various metals and alloys [48].

The thermodynamic method for determination of the nonlinear coefficient does not need the consideration of the wave profile, but it does need the control and measurement of the pressure and temperature of the sample as shown in (25), as well as premeasurement of the volume coefficient of thermal expansion μ and the specific heat at constant pressure C_p. The experimental set-up for the finite-amplitude method is relatively simple, compared to that of the thermodynamic method. However, the absolute amplitude of the vibration in the fundamental wave and the harmonic signals should be determined for the calculation of β_2 or β_3 as shown in (20) and (21). The thermodynamic and finite-amplitude methods have both been widely used for integral characterization of various media along the acoustic beam area. For applications in nondestructive evaluation or imaging of biological tissues, local properties of the materials are sometimes required, and the finite-amplitude method is preferable for these purposes. The simplest methodology assumes the lossless plane-wave propagation, so that neither diffraction nor attenuation and dispersion are taken into account for the determination of the nonlinear coefficients. A more comprehensive approach has to include the effects of dissipation, dispersion, and diffraction on the nonlinear acoustic wave propagation.

2.3. Further considerations

2.3.1. Effect of attenuation

To account for the effect of dissipation on nonlinear plane acoustic-wave propagation, we introduce thermoviscous losses into the right-hand side of the simple-wave equation (16). Since sound attenuation $\alpha \approx \omega^2$, the new term should be $\approx \partial^2 u/\partial\tau^2$, thus resulting in Burger's equation

$$\frac{\partial u}{\partial x} = \beta_2 u\frac{\partial u}{\partial \tau} + \frac{b}{2\rho_0 c_0^3}\frac{\partial^2 u}{\partial \tau^2} \tag{27}$$

Here, $b = \zeta + \frac{4}{3}\eta + \kappa\left(\frac{1}{C_v} - \frac{1}{C_p}\right)$ and ζ is the bulk viscosity, η the shear viscosity, κ the thermal conductivity, and C_v and C_p the specific heats at constant volume and pressure, respectively. The ratio of the nonlinear and dissipative terms in (27) is

$$\frac{N}{DS} \cong \frac{x_{\mathrm{DS}}}{x_{\mathrm{D}}} \equiv 2\beta_2\, Re \tag{28}$$

where $x_{\mathrm{DS}} = \alpha^{-1}$ is the dissipation distance; $\alpha = b\omega^2/2\rho_0 c_0^3$ is the attenuation factor, and $Re = \rho_0 c_0 u_0/b\omega$ is the acoustic Reynolds' number.

Therefore, when $x_{\mathrm{DS}} \ll x_{\mathrm{D}} (Re \ll 1)$ dissipation effects dominate and the contribution of the nonlinearity is small. Applying pertubation theory in this case, $u = u' + u'' + \ldots$, in the first approximation we neglect the nonlinear term in (27) and obtain the damping solution for the fundamental wave

$$u'(x, \tau) = u_0 \exp(-\alpha x)\sin\omega\tau \tag{29}$$

The second approximation yields the solution for the second harmonic in the form:

$$u''(x,\tau) = \left(\frac{\beta_2 \omega u_0^2}{4\alpha c_0^2}\right)[\exp(-2\alpha x) - \exp(-4\alpha x)] \sin 2\omega\tau \tag{30}$$

According to (30), the linear growth of the second-harmonic amplitude for $x \ll x_{DS}$ is then changed by saturation and decreased due to the dissipation effect. Formula (30) has to replace the second term in (17) for a precise determination of β_2 (and B/A) using the finite-amplitude method in solid materials, liquids, and biological media with substantial attenuation.

For $x \gg x_{DS}(Re \gg 1)$, nonlinearity dominates, however, the counterbalancing effects of dissipation result in a nearly stable shock-wave formation. Unlike the saw-tooth wave predicted for a lossless medium, in reality the shock-wave front is of a finite width ($\delta\lambda/\pi$)[12]

$$\delta = \left(\frac{1 + x/x_D}{\pi\beta_2 Re}\right) \tag{31}$$

λ is the wavelength.

2.3.2. Dispersion and nonlinearity

Frequency-dependent sound attenuation changes the $\omega(k)$ relation in a way that is equivalent to an "imaginary" dispersion. It is generally accompanied by a real dispersion, which is also characteristic of acoustic-wave propagation in relaxing media (organic solutions, semiconductor materials, etc.); waveguides; spatially nonlocal materials (liquids with bubbles, solids with microstructure); etc. To analyze the effect of dispersion on nonlinear acoustic-wave propagation, a model dispersion relation $k(\omega) = \omega/c_0 + \gamma\omega^3$ is usually introduced into the simple wave equation (16). It naturally causes the third-order derivative ($\approx \omega^3$) to appear in the right-hand side leading to the following Korteweg–deVries (KDV) equation:

$$\frac{\partial u}{\partial x} = \beta_2 u \frac{\partial u}{\partial \tau} + \gamma \frac{\partial^3 u}{\partial \tau^3} \tag{32}$$

The ratio of the dispersive and nonlinear terms in (32) is

$$\frac{DP}{N} \cong \frac{\gamma\omega^3}{\beta_2 k M_0} = \frac{x_D}{x_{DP}} \tag{33}$$

where $x_{DP} = (\gamma\omega^3)^{-1}$ is the dispersive length.

According to (33), dispersion strongly affects nonlinear propagation if $x_{DP} \leq x_D$. Stationary-wave solutions ($\partial u/\partial x = 0$) of the KDV equation range from a harmonic wave without distortion (low-amplitude wave) to a periodic distorted wave (moderate amplitudes) and soliton solutions (high amplitudes) [49]. An intense harmonic wave propagating in an ideal dispersive medium, first, tends to distort into a shocklike wave, then attains dispersive wave-front oscillations, and, eventually, falls into solitons. Losses included on the right-hand side of the KDV equation similar to the above, generally prevent solitons formation for most of acoustic materials. The effect of dispersion on the second-harmonic behavior is illustrated by the pertubation solution of the KDV equation [14]

$$u''(x,t) \approx \frac{\beta_2 k_1 u_0^2}{c_0 \Delta k} \sin\left(\frac{\Delta k x}{2}\right) \sin\left[2\omega t - (2k_1 + k_2)\frac{x}{2}\right] \tag{34}$$

where $\Delta k = k_2 - 2k_1$, $k_2 = k(2\omega)$ and $2k_1 = 2k(\omega)$.

The second-harmonic amplitude oscillates along x with the period $\Delta x = \pi/|\Delta k|$ determined by the phase mismatch between the fundamental wave and the second harmonic. As Δk increases, Δx decreases, and so does the maximum second-harmonic amplitude. This provides an additional demonstration that dispersion prevents nonlinear steepening of an acoustic-wave front.

2.3.3. Nonlinear acoustic beams

Since realistic acoustic waves are of finite aperture, the effect of diffraction on nonlinear acoustic measurements has to be taken into account. Its contribution to the right-hand side of the simple wave equation is [49] $\int (c_0/2)\Delta_\perp u \, \mathrm{d}\tau$ so that from (27) the combined effect of nonlinearity, dissipation, and diffraction is given by the following Khokhlov–Zabolotskaya–Kuznetsov (KZK) equation [13,50,51]:

$$\frac{\partial}{\partial t}\left(\frac{\partial u}{\partial x} - \beta_2 u \frac{\partial u}{\partial \tau} - \frac{b}{2\rho_0 c_0^3}\frac{\partial^2 u}{\partial \tau^2}\right) = \frac{c_0}{2}\Delta_\perp u \tag{35}$$

In (35), the high-intensity acoustic beam is assumed to be reasonably well collimated along the x-axis ($k_y, k_z \ll k$). The transverse Laplacian operator $\Delta_\perp = \frac{\partial^2}{\partial y^2} + \frac{\partial^2}{\partial z^2}$ accounts for the wave-front curvature that results from diffraction.

The ratio of the diffraction and nonlinearity contributions into acoustic-wave propagation from (35) is [12]

$$\frac{DF}{N} \cong \frac{x_\mathrm{D}}{4x_\mathrm{DF}} = \frac{D}{4} \tag{36}$$

where $x_\mathrm{DF} = \pi a^2/\lambda$ is the diffraction distance for the beam of the aperture s; λ is the fundamental wavelength.

Therefore, if $x_\mathrm{D} \ll x_{DF}$ ($D \ll 1$) the nonlinearity dominates and the diffraction contributes little to the wave-front distortion. In the opposite situation $x_\mathrm{D} \gg x_{DF}$ ($D \gg 1$), one obtains a nonlinear approximation to the diffraction problem. In this case, the second-order solution of the KZK equation shows [12] that the second harmonic always remains within the near-axis area; the 2ω beam aperture is $\sqrt{2}$ times less than that for the fundamental wave. The second-harmonic variation with distance resembles the dissipation case (see (30)): linear growth at small x is changed by saturation and subsequently decreases as x increases. However, unlike dissipation, diffraction does not prevent wave-front discontinuity, although it may be delayed to much larger distances $x = (\exp D/D)x_\mathrm{D}$.

The detailed theoretical analysis of the combined effects of nonlinearity, diffraction, and absorption in directive sound beams appeared in a series of papers, see refs. 52–55. The numerical computation code developed by Aanonsen et al. [54] has been widely adopted for a number of follow-up investigations [56–59]. Various issues, such as near- and far-field responses, dimension of sources and receivers, type of sources, and focusing beams have been considered in the studies. These theoretical results based on the KZK equation were generally in excellent agreement with experimental data in liquids and used for the development of underwater parametric arrays [7]. Later, more systematic theoretical analysis of the nonlinear interaction between acoustic beams based on KZK equations were conducted [60-63]. In these analyses different sources were modeled, including plane waves, directive beams, Gaussian beams, and their combinations, as well as consideration of different effects such as focusing, absorption, and boundary conditions. However, comprehensive investigation of the nonlinear behavior of focusing beams in solid media is still lacking in the literature, though it is very important for nondestructive evaluation (NDE) and the design of nonlinear acoustic microscopes.

2.3.4. "Nonclassical" materials

Another important consideration to be taken into account for nonlinear acoustic characterization is concerned with the specific elastic behavior of a wide class of consolidated materials like soil, cement, rocks, fluid-filled porous materials, etc. First of all, due to the granular structure the three factors analyzed above (attenuation, dispersion, and diffraction) exhibit a strong impact on elastic-wave linear and nonlinear propagation in these materials.

Moreover, the compliant properties of these materials are determined by the specific elastic forces between the structural elements that mask the classical molecular interaction and stipulate inherent

hysteresis and memory features in the stress–strain relationship [64,65]. These phenomena have a substantial effect on the material's elastic properties: elastic moduli are discontinuous functions of stress (strain) and their values depend strongly on the ambient pressure history. To simulate an elastic medium with such properties a new theoretical approach was developed by McCall and Guyer [66]. It uses the Preisach–Mayergoyz (PM) [67,68] space to describe an ensemble of mechanical states of hysteretic elements for a given pressure protocol. Once the distribution of the states in the PM space is known, one can proceed to determination of the stress–strain relationship and elastic moduli as functions of stress [69]. In the dynamic case, the discontinuity of the modulus due to the hysteresis (proportional to the wave amplitude) takes place at each fundamental wave pressure reversal. In the frequency domain, it corresponds to the higher harmonics generation with amplitudes proportional to U_0^2 [70,71], unlike the classical nonlinear material case where terms of this type are proportional to U_0^n (see (18) and (20)). Therefore, the higher harmonic generation in consolidated media can deliver the information about not only the higher order elastic moduli but also on the hysteresis-related parameters for such nonclassical materials.

3. Nonlinear acoustics for solid material evaluation

It is well known that many useful and important properties of solids have been elucidated by measurements of attenuation and velocity of acoustic waves [72]. The determination of nonlinear parameters and utilization of new nonlinear acoustic effects can provide additional valuable information that cannot be obtained by linear acoustic methods. Classical acoustic nonlinearity is a direct measure of the material anharmonicity and it delivers unique information about the nonlinear behavior of the intermolecular lattice forces [14]. The nonlinear elastic properties of solids containing micro- and macro-defects (scaled from dislocations to volume inclusions) or structural changes may be manifested in specific types of acoustic nonlinearity, which can be used as a measure of the "defectiveness" of a material or the integrity of a product structure. Despite the difference in nonlinear mechanisms, a quantitative evaluation of elastic nonlinearity of any scale and type can be achieved by measurements of the classical nonlinear coefficients introduced above or some other parameters similar to them that are always proportional to the amplitudes of the higher harmonics generated. The experimental methods most frequently used for this purpose in nonlinear acoustics are the acoustoelastic method, the finite-amplitude method, and the resonance technique. In this section we will introduce investigations based on these effects and aimed at material characterization. Due to its importance for NDE of some critical cracked defects, a special case of the nonlinear dynamic behavior of a contact interface (contact acoustic nonlinearity) and related nonlinear effects will also be considered.

3.1. Acoustoelastic method

Through the measurements of the acoustoelastic properties of a solid, the higher order elastic constants of the material can be determined. The third-order elastic constants of a solid, being phenomenological quantities characterizing acoustic nonlinearity at a macroscopic level, are also connected with the microstructural parameters responsible for its thermoelastic properties, such as thermal relaxation, thermal expansion, and conduction. They are also necessary to calculate the Gruneisen parameter showing the lattice vibration frequency dependence on the strain. Some phonon gas parameters (phonon–phonon interaction efficiency, phonon viscosity, etc.) depend on the third-order elastic constants and are of importance for a number of micromechanical properties of solids.

Hughes and Kelly were the first to measure the effect of the pressure on the sound velocity in some isotropic materials [73], while Bateman et al. [47] first determined all six third-order elastic moduli of germanium by measuring the ultrasound velocity dependence on the applied stress. Usually, the evaluation of all independent moduli requires acoustic-velocity measurements under hydrostatic pressure combined with uniaxial stresses applied. So, the key element involved in this method is the measurement of acoustic velocity with high precision [72]. Several variations of the pulse–echo technique using RF

signals interference were developed with a sensitivity to the velocity changes up to 10^{-7}. So far, the investigations of the third-order elastic constants have been carried out for a number of isotropic materials and crystals of different systems [15] with particular emphasis on hexagonal structures important for metallurgy [74]. The results of early investigations in this area can be found in several review articles [75,76].

The acoustoelastic constant defined by (26) is similar to the nonlinearity coefficient and includes all levels of acoustic nonlinearity available in the material in a quasistatic elastic mode. Therefore, it can characterize the structure of a solid at various levels: molecular, defective, structural, etc. For this reason the acoustoelastic technique has been widely used to evaluate the microstructure of metallic materials such as different carbon steels [77,78] and aluminum alloys [79–81]. It has been demonstrated that the acoustoelastic constant is sensitive to change in the volume fraction of various precipitates, such as the carbide phase in steels [77,78]; copper, magnesium, and silicon in aluminum alloys [79,81]; and hydrogen additions to a niobium single crystal [82]. The variation in temperature [83] and magnetic field dependence [84] of the sound velocity as a function of stress has also been investigated concerning its application for the characterization of metals. Recently, Nagy [85] applied the acoustoelastic effect to characterize the fatigue state in a variety of materials including plastics, metals, composites, and adhesives. Instead of applying a static load, the dynamic excitation was used to reduce the creeping-stress release and improve the accuracy of the measurements. The best fit to the experimental data was obtained by using the second-order acoustoelastic constant derived by retaining the quadratic term in the velocity–strain relation. These nonlinear constants were shown to be the earlier and more sensitive indicators of the fatigue damage than linear elastic parameters.

The technique has also been used for acoustoelastic imaging of residual stresses in metals [86,87]. It included a scanned transducer combined with accurate measurements of the acoustic-wave velocity and appeared to be an increasingly important method for the NDE of the state of the stress in structural elements. More details on this topic can be found in a recent review by Cantrell and Salama [48].

3.2. Finite-amplitude method

The third-order elastic constants can also be determined through the finite-amplitude method by measuring the nonlinear coefficients as shown in (20), (21), or (30). This method was first developed by Gedroitz and Krasilnikov [88] and Breazeale and Thompson [89]. The nonlinear coefficients or the third-order elastic constants were usually determined by measuring the second-harmonic generation efficiency or sometimes the third-harmonic signal [90] for the longitudinal waves. The finite-amplitude method can also be realized using the shear acoustic waves propagating along specific directions in crystals where their second-harmonic amplitude (unlike isotropic solids) is different from zero [91].

Gerlich and Breazeale [92] studied the relationship between the ultrasonic second-harmonic amplitude and the second- and third-order elastic moduli for different crystalline systems. The numerous calculations of the nonlinearity parameters for various crystals including piezoelectrics have been made in ref. 93. In piezoelectric materials, besides the third-order elastic constants the second-harmonic amplitude is determined by nonlinear piezoelectric, dielectric, and electrostriction coefficients. In this case the finite-amplitude method can be applied for determination of the nonlinear piezoelectric coefficients [93].

A great deal of interest has been paid to the temperature dependence of elastic nonlinearity in terms of the third-order elastic constants for various crystalline materials [15,94]. The experimental results were used for calculations of the Gruneisen parameter variation at a low temperature [15].

Recently, Na and Breazeale [95] reported the frequency dependence (in the frequency range 5–30 MHz) of the nonlinearity coefficient and abnormally high (about two orders of magnitude greater than in pure materials) third-harmonic signals in lead zirconate-titanate (PZT) ceramics. Such a behavior was interpreted theoretically [96] as the influence of dispersion and increase in the fourth-order elastic constants of the ceramics. To match the experimental data, the excess increase in the fourth-order

elastic constants, apparently caused by the granular structure of the ceramic, varied from 2 to 4 orders of magnitude for different samples.

Similar increase in acoustic nonlinearity can be brought about by other imperfections in solids and dislocations, in particular. The high elastic mobility of dislocations makes the stress–strain relation frequency dependent and essentially nonlinear. As a consequence, the second-harmonic generation for shear waves, "forbidden" for flawless isotropic materials and some crystals, was observed by Gedroitz et al. [97] in isotropic solids and aluminum single crystals. The second-harmonic amplitude was found to be highly sensitive to the stress applied to the material that confirmed the dislocation mechanism of the shear wave elastic nonlinearity.

The analogous experiment reported by Hikata et al. [98] for the longitudinal waves in a high-purity aluminum single crystal revealed about 6 dB increase in the second-harmonic amplitude under $\approx$10 g/mm^2 tensile stress. Thus, the contribution of dislocations to the acoustic nonlinearity was measured to be as much as that for lattice nonlinearity.

The sensitivity of the finite-amplitude method for shear waves has been shown to be high enough to detect the accumulation of the dislocations in the steel samples at the initial fatigue stage corresponding to periodic mechanical loads $\approx$ 10% of the safe load [99]. Conventional linear acoustic parameters used for NDE, such as ultrasonic attenuation or velocity are not expected to be sensitive to such changes of the dislocation structures.

Further investigations showed that with an increasing level of fatigue the dominant dislocation structures formed consist not only of arrays of isolated single dislocations (monopoles) but also of complex arrangements of dislocation dipoles or even multipoles [16]. The nonlinear coefficient β_2 is highly sensitive to the exact arrangement of the dislocations, which is changed under the cyclic loading. Cantrell and Yost [16] measured a 400% increase in β_2 during the first 10^4 cycles of fatigue in aluminum alloy 2024-T4, and revealed a monotonic increase in the nonlinearity parameter in stainless steel as a function of the number of fatigue cycles [100]. These results were in compliance with earlier measurements of the changes in the acoustoelastic constant of aluminum alloy 2024-T4 under fatigue cycling [29]. Thus, nonlinear acoustics provides the basis of a useful methodology for the NDE of fatigue and assessment of dislocation densities in metallic materials.

The concept of a dislocation as an area with a high local acoustic nonlinearity can be further expanded to the other disruptions in solids, such as metallic precipitate inclusion and its fraction modification, annealing and irradiating treatments, residual internal stresses, microcracks, and zero-volume disbonds. These disruptions are crucial to the quality of the metallic alloys and composite materials, and numerous investigations have demonstrated the nonlinear parameters to be sensitive to them. As shown in Table 1 [25,101,102], typical values of the nonlinear coefficients β_2 for homogeneous media fall between 1 and 10. However, experiments show that very strong nonlinear effects may be associated with the elastic properties of micro-inhomogeneous solid media ("micro" means a smallness of the structural elements as compared to the sample size and acoustic wavelength). Such a class of media includes materials that comprise grains, microcracks, dislocations, or other defects and are listed at the bottom of Table 1. The presence of these imperfections may modify the material nonlinear coefficients because of the specific elastic forces acting between the structure elements or due to the impact of the material discontinuity on the stress–strain relations.

It is well known that metallic alloys are playing more and more important roles in various fields, especially in the aviation industry. Mechanical properties of alloys are derived, at least in part, from the presence of secondary phases in the solid solution matrix [48]. The presence of the second phase, for example, raises the flow stress; and the extent of strengthening depends to the first order on the volume fraction, size, and characteristics of the second-phase precipitates formed during the manufacturing process [48]. Buck et al. [82] observed the change of the harmonic generation in a niobium single crystal with hydrogen additions. In this case, the changes to the third-order elastic constants were found to be roughly 5–10 times larger than those to the second-order elastic constants [87]. A mathematical

Table 1. Nonlinear coefficients β_2 for various media at room temperature.

Medium	Longitudinal velocity (m/s)	Nonlinear coefficient β_2
Air	340	1.2
Distilled water	1497	3.5
Ethanol	1180	5.5
Biological soft tissues	1540 (average)	3.5$\sim$ 7.0
Mercury	1450	4.9
Fused silica	5968	−3.9
Iron	5957	4.4
Copper	4759	2.4
Silver	73 704	2.0
Gold	3240	3.1
Foam plastic	$\sim$ 2000	$\sim$ 100
Marble	$\sim$ 3000	$\sim$ 800
Marine clay sediments		100 $\sim$ 1000
Rocks	$\sim$ 3000	$\approx$ 1000–10 000

model presenting the effective nonlinearity parameter of an alloy as a function of the total volume fraction of second-phase precipitates f_p, has been proposed by Cantrell et al. [103]. For f_p up to about 10%, the following linear relationship has been found to be a good approximation within experimental error:

$$\beta_2 = \overline{\beta}_2(1 + Qf_p) \tag{37}$$

The overbar denotes the values of the parameter for which $f_p = 0$, i.e., pure solid solution; Q is a coefficient depending on the linear and nonlinear constants of the pure solid solution, and the pure second-phase precipitates. Razvi et al. [80] provided experimental confirmation of (37) for the measurement of β_2 in the heat-treatable aluminum alloy (Al–Zn–Mg).

Besides the volume fraction of the second phase, the thermal treatments of alloys are also important for their material properties. Attempts have been made to evaluate aluminum alloy with different thermal aging by using the nonlinearity parameter [29,87]. The mechanism of the thermal-aging impact on the acoustic nonlinearity and strength is associated with a local coherency strain generated because of the lattice mismatch at the interface between the matrix material and the second-phase precipitate. In the early stages of aging, the increase in size and f_p of the precipitates impede the motion of dislocations and result in an increase in material strength. Further growth of precipitates leads to the loss of precipitate–matrix coherency and loss of material strength. The local coherency strain affects the dislocation network in the matrix and causes corresponding change in β_2. Numerical calculations of $\Delta\beta_2$ using the strain coherency-dislocation interaction model [104] were shown to be in compliance with experimental measurements of the correlation between variations in β_2 and the strength of the material under heat treatment [29].

Because of their practical importance in geophysics and seismology, the elastic nonlinear properties of Earth materials have been widely investigated. The compliant features of structural defects contained in rocks, such as fluid-filled cracks, grain-to-grain contacts at low pressure $P \leq 1000$ atm, give rise to a strong elastic nonlinearity demonstrated in quasistatic measurements of their acoustoelastic properties [105] and accompanied by the hysteresis and discrete memory in the stress–strain relation [64]. Dynamic

experiments using the finite-amplitude technique [106] in 2 m long rod of Berea sandstone demonstrated abnormally high value of $\beta_2 \approx 10^4$. The amplitude and frequency dependence of the second and third harmonics detected were found to be in full compliance with the classical theory predictions, (18) and (20). Further investigations in a frequency range up to 1 MHz not only confirmed the efficient higher harmonic generation for $n \geq 2$ for acoustic pulse propagation in rocks, but also revealed an extremely high contribution of cubic nonlinearity. Values of β_2 as large as $\approx 10^8$ for $\beta_2 \approx 400$ [107] were calculated from the experimental data [108] using a numerical algorithm suggested by Van Den Abeele [109].

The determination of the strength of concrete structures is very important in civil engineering. Currently, the method of estimating the strength based on the acoustic-speed measurement has received the most widespread use. However, it should be realized that in more or less homogeneous porous media the speed of the sound waves is often not a sufficiently sensitive parameter for characterizing the strength. It has been demonstrated that determination of the higher harmonics of ultrasound signals can provide a more precise evaluation of the concrete strength [34]. Another material with higher nonlinear properties is high-temperature superconductor ceramic. A comparison of the superconducting data and acoustic measurements can help to explain the role of defects, cracks, and other structural factors as well as to find the optimum technological processing regime for producing high-temperature superconductors to obtain the maximum critical currents. Dekalo et al. [20] observed that samples that were quenched in liquid nitrogen showed acoustic nonlinear behavior that was very different from samples cooled at room temperature.

3.3. Resonance technique

The finite-amplitude method works well at high ultrasonic frequencies (from 10 to 10^3 MHz) for materials with a strong nonlinearity and low attenuation ($Re \gg 1$) provided the second-harmonic growth is large enough for reasonably long distances of acoustic-wave propagation (usually tens of hundreds of wavelengths). However, the high ultrasonic damping prevents the use of this method in practically important defective materials containing serious imperfections like cracks, pores, grains, voids, etc. Instead, one can use the low-frequency acoustic waves (in the kHz or even Hz range) in a resonator configuration; the high quality factor of the resonator at low natural frequencies provides substantial nonlinearity accumulation even for low Reynolds' numbers.

The basic theory of nonlinear acoustic resonators [12] shows that an efficient higher harmonic generation takes place if the excitation frequency or its higher harmonics coincide with one of the natural frequencies of the resonator. Similar to the finite-amplitude method (see (17)), the second-harmonic amplitude is proportional to $\beta_2 M_0^2$, so that the measured ratio $u_{2\omega}/u_\omega^2$ can be used for β_2- or the third-order elastic constants evaluation.

Material acoustic nonlinearity also makes two standing waves interact, thus producing the sum- or difference-frequency spectral components in the resonator. This is a basis for the modulation version of the resonance technique developed by Zarembo et al. [110]. The shear standing wave of ultrasonic frequency ω was found to be amplitude modulated by low-frequency (Ω) pump vibrations in an aluminum rod. Mixed spectral components could be detected by making the output signal frequency coincide with one of the natural frequencies of the resonator. Its high quality factor ($\cong 10^5$) at the pump frequency Ω made it possible to detect even the double-heterodyned signal of frequency $\omega - (\omega - \Omega) = \Omega$. The method was found sensitive enough to observe acoustic nonlinear effects for Re as low as $\cong 0.05$.

The resonance technique was used by Sutin et al. [32] to observe the 10 dB increase in the second-harmonic signal due to disbonds in ceramic tiles used as thermal insulation on a space ship. The resonator comprised a tile as a mass and a felt seal as a spring and operated at the fundamental frequency of 470 Hz.

The resonance method has also been used to detect cracks in the graphitized carbon electrodes [33]. An electrode was used as a resonator with fundamental frequency $\cong$400 Hz; the second-harmonic signal was detected by a laser probe. About a 15 dB increase in $u_{2\omega}/u_\omega^2$ ratio was measured for the cracked

electrodes.

The modulation technique has recently been modified for a quantitative determination of the nonlinearity coefficient [111]. A quasistatic pump strain (ϵ_0) was induced by a vibrating ($\Omega/2\pi \cong 60$ Hz) weight attached to the resonator. Under this condition, the amplitude modulation of the ultrasonic standing wave ($\omega_0/2\pi \cong 40$ kHz) can be considered as caused by its wavelength variation near the resonance due to the change in the sound velocity:

$$V = c_0(1+\beta_2\epsilon_0) \tag{38}$$

A series expansion for small ϵ_0 yields the amplitude of the output modulated signal in the form $A = A_0(1 + m\cos\Omega t)$, where

$$m = \frac{\beta_2\epsilon_0\omega_0(\partial A/\partial\omega)_{\omega\approx\omega_0}}{A_0} \tag{39}$$

is the modulation depth. By measuring m and $(\partial A/\partial\omega)_{\omega\approx\omega_0}$, the nonlinear coefficient β_2 can be determined.

The method was applied for a quantitative evaluation of the nonlinear coefficient in steel samples subjected to stress down to tensile failure. Monotonic growth of β_2 as a function of the stress applied was observed; the maximum value of $\beta_2 \cong 10^3$ was measured in the vicinity of the sample's tensile failure corresponding to a maximum number of defects generated.

The technique was further extended to a more practical version [112], in which the pump vibrations were produced by tapping the sample with a hammer. Broadening of the output signal spectrum is obviously proportional to the material nonlinearity: for a steel sample containing a crack, the spectral sidelobes were $\cong$20 dB higher than those for a flawless sample.

Besides quadratic nonlinear effects, the higher order nonlinearity was found to manifest itself significantly in the resonance experiments. Parametric instabilities in the form of successive subharmonic generation resulting in a cascade frequency transformation nf_0/m have been recently observed [113]. Nazarov [114] used the resonance technique to study the acoustic nonlinearity of copper samples subjected to a thermal treatment. It was found that the annealing resulted in substantial increase in the third-harmonic amplitude due to the corresponding growth of the grain size in the annealed copper. The third-order effects in nonlinear resonators also result in a shift of a resonant frequency. To illustrate this effect we derive the time-averaged value of acoustic-wave velocity in solids in the third approximation, (11)

$$\overline{V} \approx c_0\left(1 + \frac{\beta_3}{6}\epsilon_0^2\right) \tag{40}$$

where ϵ_0 is the strain amplitude. Therefore, the first resonant frequency $f_0 = c_0/2L$ (L is the resonator length) will be shifted by

$$\frac{\Delta f}{f_0} = \frac{f - f_0}{f_0} = \frac{\overline{V} - c_0}{c_0} \approx \frac{\beta_3}{6}\epsilon_0^2 \tag{41}$$

By measuring the nonlinear resonant peak shift one can calculate β_3. Experiments in the 0.5–1.5 kHz range with resonators of rock [115] revealed frequency shifts of 10% or more over strain intervals 10^{-7}–10^{-6} accompanied by dominant third-harmonic generation. Calculations of β_3 from the third-harmonic amplitude detected, showed surprisingly high values for various rocks: $\beta_3 \cong 10^{-10}$–10^{-15}. Moreover, unlike (41) $\Delta f(\epsilon_0)$ was found to be proportional to $\epsilon_0^{0.7-1.5}$ for various materials with the power index decreasing at larger strain. These observations do not comply with predictions of classical nonlinear acoustics and are assumed to be associated with such important features of rocks as the elastic

hysteresis and end-point memory [24]. An enormous nonlinearity discovered in rocks may affect many areas in seismology and be used to monitor the important material parameters in rock mechanics.

In conclusion, we note that the results obtained by different authors and presented through the last two subsections unambiguously demonstrate a strong correlation between the acoustic nonlinearity coefficients and the generation and growth of the defects in the materials, i.e., their strength degradation. Therefore, the measurements of $\beta_{n\omega}$ provide unique information on the material strength and can be used to predict its failure far in advance.

3.4. Nonlinear NDE using contact acoustic nonlinearity

This subsection will be concerned with nonlinear acoustic methodologies applicable to the characterization and location of various fractured inhomogeneities and defects in solids. The characteristic element of such inhomogeneous inclusions as pores, cracks, grains, structural frames, etc. is an internal interface separating the intact material and the inclusion. Generally, it is supposed to be the contact interface, i.e., the interface that is either free (large pores, opened cracks), partially clamped ("clapping" contact of closed cracks, zero-volume unbonds), or ideally bonded. A thorough study of acoustic nonlinear phenomena for such contact interfaces (contact acoustic nonlinearity (CAN)) is needed to evaluate the nonlinear properties of the defects and to develop new methods for their detection and characterization.

For the ideally bonded interface, a general approach to the boundary acoustic nonlinearity (nonlinear reflection technique) was first developed by Shui and Solodov [116]. It was shown that generally all the waves existing at the interface contributed into the interface acoustic nonlinearity. Therefore, even "linear" propagating acoustic waves (for example, the shear waves in an isotropic solid) efficiently generate higher harmonics in reflection and transmission at the interface. For a free boundary of a piezoelectric crystal, one can expect nonlinear contribution of all four electroacoustic modes into the second-harmonic reflected field [117]. In other words, even for a weakly nonlinear incident acoustic wave, interaction with the interface can result in a strong nonlinear reflection and transmission, i.e., an efficient reflected and transmitted harmonic generation. The theory was later extended to include the analysis of the reflected and transmitted second-harmonic fields for an anisotropic interface [118] and polarization effects accompanying nonlinear shear wave reflection [119]. The relation between the amplitude of the reflected second harmonic ($U^0_{2\omega}$) and the incident fundamental wave (U_0) was shown to be as follows [120]:

$$U^0_{2\omega} = \frac{\beta_{\mathrm{R}}}{2} k U_0^2 \tag{42}$$

The nonlinear reflection coefficient β_{R} depends on the linear and nonlinear constants of the adjacent materials and increases greatly for angles of incidence over critical angle. According to experiment [120,121], for shear wave reflection from typical nonlinear materials, β_{R} ranges from $\cong$10 to $\cong 10^3$. According to theory, $\beta_{\mathrm{R}} \neq 0$ even when a linear acoustic impedance is continuous across the interface; therefore, the reflected second harmonic is generated when there is a lack of a linear reflection. This demonstrates a unique opportunity for nonlinear detection of the inclusions "invisible" with conventional (linear) acoustic instruments.

This conclusion has been experimentally confirmed for the shear wave reflection at a partially clamped contact interface [122] between two highly polished samples of glass. The increase in the contact compression load naturally causes the amplitude of the fundamental reflected wave to decrease drastically (transmission through the contact increases). Meanwhile, despite the fact that glass is quite a linear material for shear waves, a very efficient higher harmonic generation (up to the fourth) was observed from the contact area. The amplitudes of the harmonics were strongly dependent on the contact load and reached maximum for the ambient pressure $\approx$1–2 MPa.

The mechanism of such a high contact nonlinearity was demonstrated in a simulation experiment [123]. The spectrum and temporal forms of low-frequency vibrations were recorded for different amplitudes of the signal driving a partially clamped contact. A threshold distortion of vibration forms and the

higher harmonic spectrum enrichment were found to be caused by "clapping" of the contact surfaces. Consecutive "opening" and "closure" of the contact was proved to be a highly nonlinear process, which features not only a strong superharmonic generation with non-monotone spectra, but also a number of subharmonic and quasichaotic dynamics [123]. The experimental results on the second-harmonic generation due to CAN were in excellent agreement with the first theoretical predictions by Richardson [124]. These results explain anomalously efficient higher harmonic generation in the reflection at the contact interface observed in ref. 122; one should expect similar highly nonlinear behavior for acoustic waves in materials with fractured defects and cracks.

The theoretical analysis of the nonlinear contact problem was continued by Achenbach and Norris [125], who investigated the reflection and transmission of an incident wave by an infinite flaw plane. The interaction of the faces of the flaw was modeled by the nonlinear relation between the crack–face tractions and the crack-opening displacements. The dynamic problem of contacting crack faces because of incident wave motion has been solved numerically by using the boundary element method [126]. The relationship between the harmonic generation efficiency and the degree of crack-opening displacements with varying external stresses was investigated numerically. Some other models for crack dynamics caused by an acoustic wave have also been proposed [127,128].

Besides the clapping mechanism, a nonplanar contact interface (closed cracks with rough surfaces) can also exhibit Hertzian nonlinearity [129]. Since the area of the nonplanar contact changes during deformation, a compressive load (F) applied to such a contact (two spheres of equal radii R) is the nonlinear function of strain (h) given by the following relation [129]:

$$F = Kh^{3/2} \tag{43}$$

where $K = (R/2D^2)^{1/2}$ is the effective elastic constant, which depends on the asperity radius and material elasticity (D). In the dynamic case under static load $h = h_0 + h_\omega$, where h_0 is the static strain of the contact. Substituting this expression for h into (43) and using a Taylor-series expansion for $h_\omega/h_0 \ll 1$ we obtain the dynamic stress–strain relation. Using the definition of β_n (see (10)) as a negative normalized coefficient of the nth-order term in this relation we obtain

$$\beta_2 = \frac{1}{4h_0}, \qquad \beta_3 = -\left(\frac{1}{24h_0^2}\right) \tag{44}$$

According to (44), one may expect a substantial nonlinearity of the nonplanar contact for low static loads accompanied by particular increase in the third-order effects. The experimental results [31] proved the contribution of the Hertzian mechanism into CAN to be the highest for weakly pressed contacts. Generally, as the contact pressure decreases, the contact vibrations first turn into a mixed mode, where the clapping nonlinearity is combined with the Hertzian mechanism followed by a domination of the clapping contribution. However, for rough surfaces in contact, a diversity of radii and heights of asperities results in a successive clapping of microcontacts, thus broadening the threshold transition to the clapping mode. As a result, the width of the contact load range, in which the CAN exhibits maximum is proportional to the surface roughness. Experimental measurements of the second-harmonic amplitude as a function of the contact pressure for the shear wave reflected from a rough glass–glass interface [31] have confirmed the viability of the new method for the surface roughness evaluation.

A theoretical model of the CAN based on the rough contact representation as an ensemble of springs with different lengths developed by Rudenko and Wu [130] made it possible to adopt the method for a quantitative determination of the asperity height statistics. A similar theoretical approach was used in ref. 32 to characterize the acoustic nonlinearity of the materials with cracks. The authors derived the expressions for linear elasticity (α) and the second-order nonlinear coefficient (β_2) of a single crack

$$\alpha = \frac{\pi h_s R^2 (E/\sigma_0)}{(1 + h_s/d_0)} \tag{45}$$

$$\beta_2 = \frac{\pi h_s R^2 (E/\sigma_0)^2}{(1+h_s/d_0)^3} \tag{46}$$

and the overall nonlinear coefficient for the material with crack concentration N_0:

$$\epsilon = \left(\frac{5\beta_{20}N}{16}\right)\left(1+\frac{3\alpha N_0}{8}\right)^{-2} \tag{47}$$

In the formulas above, E is the Young's modulus for the intact material; R is the diameter of the crack, which is assumed to be of a round shape; h_s the effective height of the roughness for each rough surface of the crack; d_0 the distance between the middle lines of the rough surfaces; and σ_0 is the static compressive stress applied to the crack.

Numerical estimations for $N_0 = 20$ cm^{-3} and typical values of the crack parameters, demonstrated an increase of about two-orders of magnitude in ϵ as compared with the nonlinear coefficient of the intact material. Note, that such an increase (however, somewhat less substantial) was observed in the early experiments of Buck with co-workers [131,132] and recently confirmed by Nagy [85] for fatigue cracks.

The CAN also has an effect on the surface acoustic-wave (SAW) propagation that can be used for the characterization of the nonlinear surface and interface. An efficient higher SAW harmonics generation in the CAN area was reported in ref. 122. The following values of the CAN nonlinear coefficients (for the second- and third-order, respectively,) have been obtained from these experimental data [31]:

$$\beta_2 \cong 50, \qquad \beta_3 \cong 7\times 10^4 \tag{48}$$

The value of β_2 in (48) is in a fair agreement with $\beta_2 \approx 100$ calculated from formulae (44) for a single crack of the same size as the CAN area and other contact parameters used in the experiment [122]. According to Sect. 2.1, in the classical nonlinear acoustics of homogeneous materials the quadratic nonlinearity dominates and $\beta_3 \cong \beta_2^2$, (19) and (20). From (48): $\beta_3 \cong 30\beta_2^2$, therefore CAN demonstrates an abnormally high level of cubic nonlinearity. Taking into account similar results described for the cracked rocks and granular ceramics in Sects. 3.2 and 3.3, one can conclude that the cubic nonlinearity domination is a general feature of all materials containing contact interfaces. The "nonclassical" character of CAN is due to a discontinuous behavior of the material elasticity that has certain similarity with the hysteretic nonlinearity discussed in the previous sections. Specific harmonic contents provided by CAN is manifested in an unconventional nonlinear wave-form distortion ("rectified" sine) obtained by numerical calculations by Hirose and Achenbach [126] and observed in the experiments for both bulk and surface waves [122,31].

The CAN area, behaving like a crack and possessing the high β, $\beta_{3\omega}$, represents an abrupt nonlinear inhomogeneity for an incident SAW. Similar to the bulk wave case considered above, one should expect an efficient nonlinear acoustic reflection. The experimental results demonstrated dramatic backward higher harmonic generation from the CAN area [133]; in compliance with (49) the reflected third harmonic was generated much more efficiently that the second one. Moreover, since linear reflection at the contact is usually small, a unique feature of "spectrum inversion" in the nonlinearly reflected SAW ($U^R_\omega < U^R_{2\omega} < U^R_{3\omega}$) was observed for intense incident SAW [133,134]. In terms of NDE and imaging, this means that for cracked defects the acoustic contrast of the defect image is expected to grow along with the number (n) of the specific harmonics selected in the reflected field. A physical interpretation of this fact is as follows: the object reflectivity of the nth order is assumed to be proportional to the ratio of the $(n+1)$th-order elastic constants for the defect (d) and intact material (m) [135]. Since for the latter typically (see Table 1) $(\beta_{2\mathrm{m}}) \le 10$, $(\beta_{3\mathrm{m}}) \le 100$, while the linear reflection from the CAN area is negligible, by comparing with (48) we obtain

$$\frac{c^{\mathrm{II}}_{\mathrm{d}}}{c^{\mathrm{II}}_{\mathrm{m}}} \cong 1, \qquad \frac{c^{\mathrm{III}}_{\mathrm{d}}}{c^{\mathrm{III}}_{\mathrm{m}}} \ge 5, \qquad \frac{c^{\mathrm{IV}}_{\mathrm{d}}}{c^{\mathrm{IV}}_{\mathrm{m}}} \ge 700 \tag{49}$$

that clearly shows the advisability of the nonlinear reflection mode NDE for the cracked inclusions.

Various modes of the nonlinear NDE were tested [31] to detect the fractured surface defects. In the nonlinear transmission mode, the integral increase in β_2 over the path of a SAW propagation was measured in the presence of defects. Similar results reported earlier for the bulk acoustic waves [131,132] were used for a qualitative evaluation of the fatigue-crack development. The nonlinear reflection mode was studied for $n = 1$–3 and revealed dramatic contrast improvement as n increased [135,136]. This also made possible the recognition of the degree of fracture (proportional to the reflected harmonic amplitude) as well as the location of a defect (output pulse delay). The viability of the nonlinear tomography mode was demonstrated using the nonlinear interaction of contra-flowing SAWs resulting in double-frequency bulk wave generation [137]. The scheme was shown to perform one-dimensional scanning of CAN distribution along the defective surface area reconstructing a plane of a tomographic image [138].

Another important application of the CAN in NDE is concerned with the adhesion quality control. Conventional (linear) acoustic NDE instruments are used for detecting the areas of a weak adhesion strength or complete delaminations, while incomplete adhesion ("kissing" contacts) or zero-volume disbonds are beyond their capability. The CAN phenomena are particularly applicable to these situations, and the NDE modes proposed above can be naturally adopted to monitor the strength of bonding.

The feasibility of the nonlinear transmission mode use for the quantitative adhesion strength characterization with bulk acoustic waves has been studied by Fassbender et al. [30]. The following parameter was derived to represent the adhesion strength assuming that the distortion of ultrasonic waves mostly occurs in the binding interface:

$$S = A_1 - A_2 + A_3 - A_4 + \ldots = \sum_{i=1} (-1)^{i+1} A_i \tag{50}$$

where S is the parameter indicating the adhesion strength and A_i ($i = 1, 2, 3, ...$) are the amplitudes of the fundamental frequency component its higher harmonics.

According to (50), to evaluate the adhesion strength one has to measure the transmitted acoustic-wave spectrum. In experiment, a pulse of the intense longitudinal wave was generated by a narrow-band transducer. The transmitted wave was received with a broad-band transducer and the FFT was used to calculate its spectrum and the adhesion strength from (50). A good correlation was demonstrated between S calculated and actual adhesion strength determined by the mechanical method [30].

In this section, we have reviewed some applications of nonlinear acoustics for the characterization of solid materials. They covered the defects in different levels, including lattice structure of crystals, dislocation in metallic materials, alloy volume fraction, microcracks in various materials, and disbonds. Most of the methods introduced in this section make it possible to characterize the integral nonlinear properties of media. In the next section, the experimental techniques involved in the nonlinear acoustic investigations will be introduced followed by the methods for nonlinear acoustic imaging and the determining a position of a local defect.

4. Experimental considerations

Before introducing methods for locating and imaging defects using nonlinear acoustics, we will first summarize the experimental configurations and detection methods for nonlinear acoustic studies in various media.

4.1. Experimental arrangements

The layouts of various nonlinear acoustic experiments concerned with material characterization are summarized in Fig. 1.

In Fig. 1, the arrangements of the transmitting and receiving ultrasonic transducers with the specimen are highlighted. The data on the other elements of the experimental set-ups, such as parameters of electronic components, mechanical driving devices, etc. can be found in the references of the preceding sections. Figure 1 covers the methods for probing the acoustic nonlinearity of the materials introduced above, i.e., the thermodynamic (for liquids) or acoustoelastic (for solids) method, finite-amplitude method, resonance technique, as well as acoustic-wave interaction. The longitudinal (focused and unfocused) and shear bulk waves, surface acoustic waves, and interface waves (Stoneley-type) have been adopted for the study of material nonlinear properties. An introduction to each experimental scheme is given in the following subsections, and its potential in nonlinear NDE is also proposed.

The nonlinearity of the material can be represented as the relationship between the acoustic-wave velocity and the applied static load. Figures 1*a* and 1*b* demonstrate the layout of this method in solids and liquids. Figure 1*a* illustrates the determination of the acoustoelastic relationship between the changes of the acoustic velocity and the load applied to solid samples [47]. A single transducer is used and the ultrasonic reflection mode is adopted. This method has been extended to obtain the image of stress distribution in a sample with the applied load [86]. The transducer is scanned along two directions of the sample surface; the 2D-stress distribution is derived from the acoustic velocity variation as a function of the coordinates.

Figure 1*b* demonstrates the thermodynamic method for determination of the nonlinear parameter B/A in liquids [139]. The temperature and the pressure of the sample are controlled and measured. According to (25), the B/A parameter can be determined by measuring the change in the ultrasound velocity with temperature under the constant pressure, and $\partial c/\partial p$ under isothermal conditions. The improved thermodynamic method proposed in ref. 140 makes use of the direct isentropic measurements of the sound speed variation with pressure rather than using an isothermal process. The key element for both the thermodynamic or acoustoelastic measurements is the determination of the sound velocity changes using the techniques introduced in Sect. 3.1.

The acoustic nonlinearity of materials can be determined by the finite-amplitude (or spectral) method. The finite-amplitude acoustic wave is generated in media with a transducer. The wave will be distorted and the higher harmonic signals will be generated during its propagation. The distorted acoustic wave is then detected with a broadband transducer or a transducer with the specific frequency response can be used to receive the higher harmonic signals. By using a broadband transducer, the amplitude of each harmonic can be calculated through the FFT analysis of the received signals. By measuring the amplitudes of the received fundamental wave, its second- and third-harmonic signals, the nonlinear coefficients β_2 and β_3 can be determined using (21) and (20).

Figure 1*c* gives another version of the finite-amplitude method for the measurement of the acoustic nonlinearity of liquid and biological media (finite-amplitude insert-substitution method) [140]. The specimen is placed in a container that is covered by film on two sides. By comparing the amplitudes of the second-harmonic signals obtained for the sample liquid and for a liquid with known nonlinear parameter, the B/A of the sample liquid can be derived. This method does not need the measurement of the absolute value of the acoustic-wave amplitude and enables us to account for the effect of both sound attenuation in the samples and diffraction of the transducer on the acoustic measurements.

Similar experimental arrangements, which use focused acoustic beams have also been proposed for the determination of the nonlinear parameter of liquids [141], see Figs. 1*d* and 1*e*. The transmitted acoustic waves are focused using an acoustic lens and the harmonic signals are received by plane transducers after the focused beams have passed through the liquid sample. Since the nonlinear effects can be assumed to occur only in the focal zone, the focused beam techniques can be used to characterize the nonlinearity of a very small amount of liquid, especially in the scheme shown in Fig. 1*e*, where a sample container with film on the sides is arranged.

Various experimental configurations have been proposed for investigation of the bulk nonlinear acoustic properties of the solids as well as their boundaries and interfaces. Figure 1*f* shows the ar-

Fig. 1. (*a*)–(*m*) Experimental configurations used for acoustic investigations of material nonlinear characteristics. (*Figure 1 is concluded on the facing page.*)

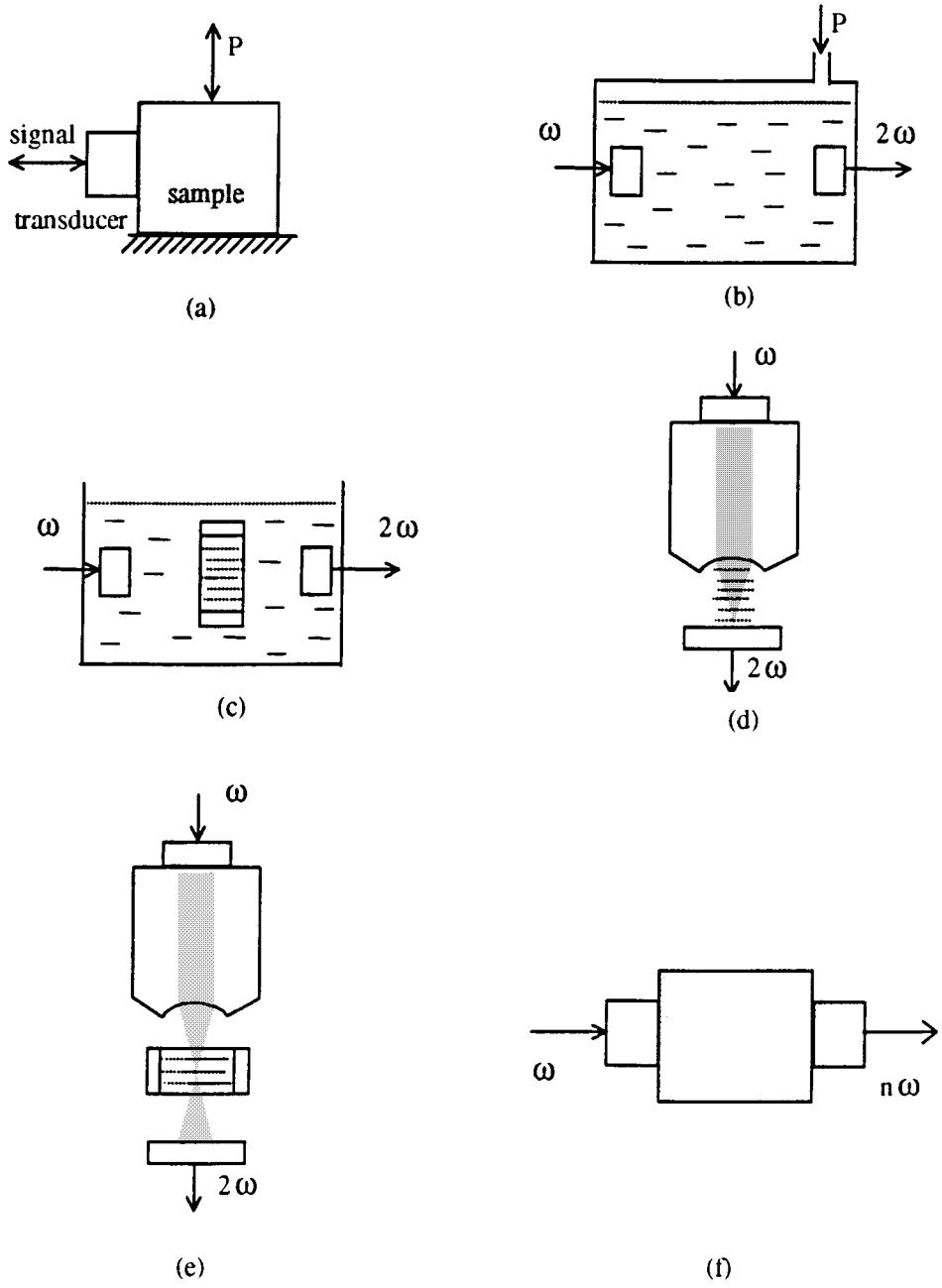

rangement for determination of the acoustic nonlinearity coefficients in solid samples by using the finite-amplitude method in homogeneous media on the basis of (20), (21), or (30). A similar scheme can be used for the characterization of inhomogeneous materials as well. In this case, an abnormally high amplitude of the higher harmonics in the sample is a qualitative indication of the presence of various

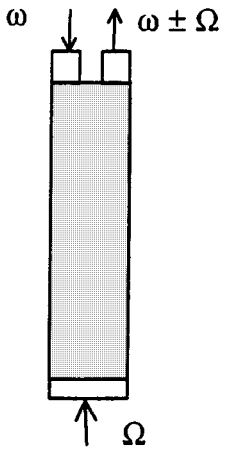

(g)

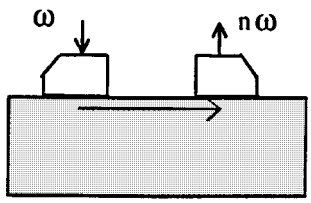

(h)

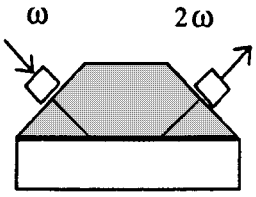

(i)

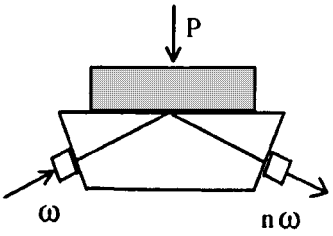

(j)

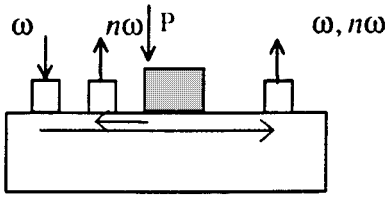

(k)

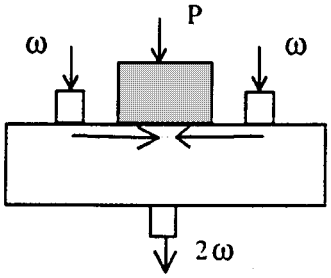

(l)

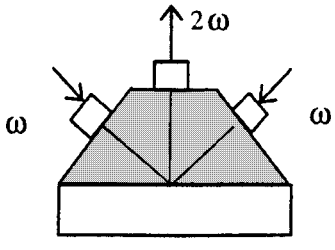

(m)

defects in the sample, such as disbonds [30], cracks [131], etc. A quantitative analysis of these types of flaws can also be implemented on the basis of (50) for the disbonds and (47) for the crack defects.

The modulation technique arrangement is illustrated in Fig. 1*g*. Piezoelectric transducers or accelerometers are used to detect the mixed frequency signals. The length of the sample is chosen to provide natural frequencies close to the driving frequency. Equation (39) is applied for a quantitative determination of the material nonlinearity. The other versions of the resonance technique in Fig. 1*g* include the higher harmonic detection or the measurements of the sample resonant-frequency shift as a function of a single driving source amplitude.

The experimental arrangements introduced above usually make use of the longitudinal wave, and are commonly described in the literature. The other types of acoustic waves, such as shear waves, surface acoustic waves (Rayleigh-type), and Stoneley-type waves are also adopted in the investigation of acoustic nonlinearity in solid media. Compared to the bulk waves, SAWs are particularly suitable for investigating the nonlinear interactions since the energy of a surface wave is confined to approximately one acoustic wavelength from the surface and the energy density is high due to a small subsurface penetration of the wave [142]. For this reason, the nonlinear effects can be observed at a much lower driving voltage than that in the bulk wave experiments. To generate SAWs, the wedge transducers are normally used for isotropic solids; the interdigital transducers represent the most efficient means for producing the finite-amplitude SAWs in piezoelectric materials.

Monitoring SAW higher harmonic amplitudes as a function the distance between the transducers in Fig. 1*h* (or using the optical probing) makes a flexible determination of both the dissipation and dispersion contributions into the SAW harmonic generation possible. Because of the lack of dispersion, the finite-amplitude method, which uses SAWs, can be applied for a quantitative determination of β_2, or the third-order constants, using the analytical expressions for the SAW second-harmonic amplitude obtained in ref. 116 and modified (if needed) to account for the attenuation from (30).

Unlike bulk acoustic waves, the SAW dispersion is quite common and usually caused by the material subsurface inhomogeneity, which reflects the technological "history" of the sample (grinding, polishing, cold-work, etc.). As indicated in Sect. 2.3, the presence of the dispersion will be manifested in the oscillations of the SAW second-harmonic amplitude along the propagation path. Therefore, by measuring the period of oscillations in accordance with (34), one can easily evaluate the appearance of the surface inhomogeneity (layers, films, etc.) due to technological operations or even proceed to its quantitative analysis. Equation (34) can also be used for determining β_2 by the finite-amplitude method in dispersive media. The surface microcracks and other fractured defects can also be identified by the increase in the second-harmonic amplitude [31] in the SAW nonlinear propagation mode shown in Fig. 1*h*.

The nonlinear interface-wave (Stoneley wave) analysis presented in ref. 116 makes possible the application of the finite-amplitude method for the evaluation of nonlinear parameters of the adjacent materials. Figure 1*i* shows the scheme, which has been used to study the nonlinear behavior of the interface wave between two solid media [143]. The wedge technique was used to generate the fundamental interface wave, which generally turned out to be a leaky interface wave. The Stoneley wave exists only on the interface between some specially selected materials; its nonlinear propagation mode [144] has a potential for evaluating the bonding conditions of the interface.

The experimental configuration of the nonlinear reflection mode shown in Figs. 1*j* and 1*k* have been used to study the contact acoustic nonlinearity [31] using bulk and surface acoustic waves. The bulk-wave version (Fig.1 *j*) uses both the vertically and horizontally polarized shear waves [120,145]. Since no shear second harmonic is generated in isotropic solids, the substrate nonlinearity can be neglected in Fig. 1*j*. For a high contact load P, the measurements of the nonlinear reflection coefficient introduced by (42) were shown to have a good correlation with the nonlinear properties of the overlying materials. This configuration is also applicable to a quick test of acoustic nonlinearity induced by the defects in the overlaid materials. Some new information about nonlinear material properties can be obtained

by measuring the polarization of the second harmonic generated in the reflection of the shear wave [145,119].

In the range of intermediate loads, the CAN contribution to the output signal in Fig. 1*j* is dominant and the acoustic harmonics observed simulate nonlinear behavior of the cracked defects. In a practical context, the configurations in Figs. 1*j* and 1*k* are suitable for the nonlinear NDE of the disbonds and interface cracked defects "invisible" with linear acoustic diagnostic equipment [31]. The delay of the "reflected" higher harmonic signal in both schemes provides the information on the position of the defect or disbond along the propagation path of the incident wave. The SAW nonlinear reflection mode Fig.1*k* was reported to be used for the nonlinear NDE of the cracked defects on the surface of $LiNbO_3$ substrate [146]. The scheme, Fig. 1*j* was also used for a qualitative and quantitative [130] nonlinear NDE of the surface roughness.

The configuration, which uses combined surface-bulk wave nonlinear interaction, is shown in Fig. 1*l*. It employs nonlinear interaction of the contraflowing SAWs of equal frequency in the partially clamped contacts. The amplitude of the double-frequency bulk wave generated into the interior of the substrate is used as an indication of the CAN efficiency [137]. When one of the input SAWs is a short pulse, the output second-harmonic signal as a function of time represents the one-dimensional distribution of the CAN along the SAW propagation path. In particular, such a scheme is advantageous for real-time scanning of the adhesion strength of the contacts. This configuration was used to scan the distribution of the fractured defects on the free surface of the substrate [138].

Figure 1*m* uses the obliquely incident fundamental bulk waves instead of the SAWs [120,143]. Similar to the surface-wave counterpart (Fig. 1*l*), it performs the nonlinear acoustic NDE of the interface and evaluation of the interface bonding. The experiments in Figs. 1*l* and 1*m* also represent a basis for nonlinear tomography schemes applicable to subsurface defective areas. These two configurations supplement each other in terms of the scanning capabilities: for a fixed angle of incidence (including $\pi/2$ as a degenerate SAW case), the incident acoustic pulse "reads" the subsurface nonlinear properties along certain direction; in principle their combination enables us to reconstruct a tomographic 2D-image of a nonlinear inhomogeneity.

In summary, four principle experimental methods are in use for acoustic nonlinearity characterization of a wide range of solid and liquid materials: the thermodynamic, acoustoelastic, finite-amplitude, and resonance techniques. The methods employ various types of bulk, surface, and interface acoustic waves and provide information ranging from lattice anharmonism to the presence of defects. The acoustoelastic and resonance techniques are less affected by attenuation in solids, so they are advantageous for use on imperfect (constructional, defective, etc.) materials. In this case, the nonlinear reflection mode is helpful to detect the disbonds or fractured microdefects that are invisible with conventional linear acoustic instruments. In terms of the defect locating, the opportunities for tomographic nonlinear imaging are created by using the configurations based on the three-wave acoustic interactions. The issue of the nonlinear imaging will be further considered in Sect. 5.

4.2. Detection methods in nonlinear acoustics of solids

Most of the nonlinear acoustic experimental configurations of Fig. 1 feature "nonreciprocal" detection — the frequency of the receiver is different from that of the transmitter. The detected acoustic-wave frequency transformation is an indication of the nonlinear behavior of the transmitted wave; the information on the nonlinearity of the material is obtained by analyzing either some specific spectral components or the overall spectrum of the output signal. Therefore, the nonreciprocal (superharmonic, subharmonic, broadband, etc.) detection is one of the challenges for a nonlinear acoustic experiment.

Another issue is related to the sensitivity of a detection method. Since the driving power applied to the transmitting transducer is limited by the linear response of the piezoelectric material and electrical circuits, the nonlinearly generated harmonic signals in a typical sample are considerably small. Moreover, this is an intrinsic condition for the fixed-field approximation, in which the basic equations (18),

Fig. 2. (*a*)–(*c*). Acoustic wave forms used for nonlinear acoustic experimental investigations.

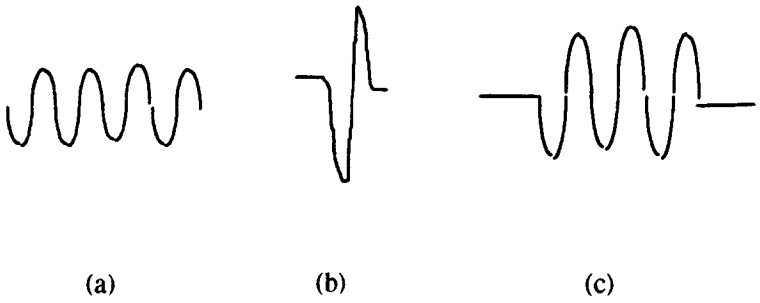

(20), and (24) are valid, binding the experimental data and material nonlinear parameters. For example, a 10 MHz, 40 A, 6000 m/s longitudinal acoustic wave propagating 1 cm distance in a material with the nonlinearity coefficient β_2 of 2.5, develops a 20 MHz second harmonic with an amplitude of $\approx$0.1A [19]. The displacement of the higher harmonics will be much lower; for example, the amplitude of the third harmonic can be as low as 0.001A [90]. Assuming average $\cong$ 20 dB insertion losses introduced by each of the transmitting and receiving transducers, we find that a typical experimental set-up for nonlinear acoustic research should manage an input/output voltage ratio not less than $\cong$ 20–100 dB.

Finally, unlike linear acoustics, the absolute values of the wave amplitudes are generally required for a quantitative analysis of the nonlinear acoustic experiments. This is illustrated by (20), (21) where the ratio of the higher harmonic amplitude to the square or cube of the fundamental wave amplitude is needed to evaluate β_2, β_3. Since different detecting transducers are to be used in ω and $n\omega$ circuits (or the sensitivity of a broadband transducer is different at those frequencies), the relative (voltage) measurements are not enough to calculate β_2, β_3 and the higher order coefficients.

Before proceeding to specific detection methods, which satisfy the above requirements, we briefly introduce the wave forms adopted in the nonlinear acoustic experiments (Fig. 2). Using the continuous-wave mode, single-frequency generation can be achieved, which is a very important condition for the investigation of the acoustic nonlinearity. In addition, a sensitive phase-detection method can be adopted to detect the frequency or phase change in the received continuous signal [147]. Furthermore, a continuous wave is used to generate standing waves in a resonator configuration and is a necessary element for the resonance technique realization. However, a high power continuous wave is usually difficult to achieve, the mode is not time-selective and that aggravates the issue of direct feedthrough signals and makes it impossible to locate the defects.

Nonlinear acoustic investigations using the pulse mode are attracting more and more interest, since this mode is the most suitable for practical applications of nonlinear acoustics in biomedical imaging, NDE, and acoustic microscopy, where spatial resolution is crucial [148,149].

Similar wave forms of high-intensity are usually generated in laser acoustics [150]. The nonlinear acoustic properties of the media are derived from the distortion of the pulse, which can also be affected by the frequency-dependent attenuation, diffraction, etc. Numerical methods for the finite-amplitude acoustic-wave propagation have been developed to handle the pulse signal, which is rich in frequency components, and to take into account the frequency-dependent attenuation [151]. The situation can be more complicated due to the fact that the frequency components of the acoustic pulse can interact with each other while the wave passes through nonlinear media.

According to the literature for these reasons, the tone burst (RF pulse) mode, which is the compromise between the continuous wave and pulse modes, has been commonly used for nonlinear acoustic investigations. In this mode, the high output power can be combined with the narrow frequency band

Table 2. Comparison of basic properties for detection methods adopted in nonlinear acoustics.

Detection method	Sensitivity	Frequency response	Contact condition	Absolute value	Surface preparation	Limitation
Capacitive	High	Broadband	Semicontact	Easy	Most critical	Precise alignment
Piezoelectric	High/ medium	Narrow	Contact	Difficult	Casual	Narrow frequency band
Optical	Medium	Broadband	Noncontact	Difficult	Critical	Optical system
Electrodynamic	Medium	Broadband	Contact	Easy	Casual	External magnetic field
Accelerometric	Low	Low frequency	Contact	Difficult	Casual	Low frequency

of the signal and reasonable time resolution. The tone burst mode has been adopted in most of the early investigations of the acoustic nonlinearity in solid media [15].

In a nonlinear acoustic experiment, care should also be taken to choose the ultrasound transducer driven by one of the signals introduced above. The transmitting transducer is to provide acoustic vibrations intense enough to induce nonlinear effects in the media and meanwhile ensure that the acoustic signal is not distorted by the nonlinearity of the piezoelectric materials or the electrical circuits before it is transmitted into the media. Quartz or lithium niobate transducers are usually selected for nonlinear acoustic study because of their high efficiency and rather linear response (unlike the piezoceramic transducers) [87].

For different applications, five methods can be distinguished, which according to the literature, are used for the detection of nonlinearly generated acoustic signals. They use the capacitive receiver, piezoelectric transducer, optical probe, electrodynamic transducer, and accelerometric detector. Their basic properties are summarized in Table 2.

The capacitive detection method was used for the investigations of the finite-amplitude longitudinal acoustic-wave distortion in various materials [15]. While using this method, the surface of the sample is first carefully polished, and then a metallic film is deposited on the sample face (for nonmetallic materials). This surface acts as one side of a capacitor, while the other side is formed by a detecting electrode placed at some distance from the sample face and connected to the electronic circuits. A bias voltage is applied between the capacitor plates. The ultrasonic vibrations of the sample face cause variations in the capacitor gap spacing and hence the voltage across the capacitor. The output voltage is directly proportional to the displacement of the surface, and is weakly dependent on the frequency. After calibration at the fundamental frequency and higher harmonics, the capacitive detector can provide the absolute amplitudes of the surface vibrations produced by the corresponding spectral components. By using the capacitive detector, the measurement of amplitudes as small as $10-4$A is possible [15]. A high sensitivity and broadband-frequency response make it suitable for the study of the nonlinearly generated high-order harmonics in various solids. Since the capacitor gap spacing is usually $1 \sim 5\ \mu$m for a high sensitivity, the sample should be optically flat over the receiving area, which is about 1 cm^2. For this reason, the sample preparation, capacitor arrangement, and precise (optical) alignment of the assembly are crucial in the capacitive detection method.

The piezoelectric detector using a transducer of a piezoelectric material (quartz, $LiNbO_3$) is the most commonly adopted method for nonlinear acoustic investigation in various media. It is much simpler,

more reliable, and practically more acceptable than the capacitive receiver. At a resonant frequency its sensitivity is comparable with that of the capacitive detector, however, providing a narrow frequency band. This mode of operation can be used only for the detection of a single selected harmonic of an output signal. The broadband mode is also possible at the expense of the sensitivity degradation; if the resonant frequency of the detector is much lower than the fundamental-wave frequency, its frequency response in a high-frequency range is rather flat, which makes the observation of nonlinearly distorted wave forms possible [8]. The ultrasound transducers with a wide range of frequencies and sensitivities are commercially available with industrial standards. Similar to the capacitive detector, the piezoelectric transducers, in principle, provide absolute-amplitude measurements; however, preliminary determination of the transducer insertion losses and the parameters of its equivalent circuit are required.

In the SAW nonlinear experiments, piezoelectric interdigital transducers (IDTs) are usually employed to detect the higher SAW harmonics. They feature a very high sensitivity (insertion losses several dB) and adjustable bandwidth (up to $\cong$ 100%), which is, however, not sufficient for the detection of the SAW nonlinear distortion. A piezoelectric point probe comprising a metal needle placed at some distance above a piezoelectric substrate was successfully used for this purpose [152].

Another point-type detector employs the acousto-optical interaction that had been widely used for laser-beam deflection and modulation as well as acoustic-wave detection in liquids and solids [153,154]. It is based on the fact that the intensity of the light diffracted (to the first-order maximum) by a bulk acoustic wave (in a small amplitude approximation) is proportional to its acoustic power. If the material photoelastic constants are known, the measurements of the diffracted light intensity enables determination of the absolute values of the acoustic-wave displacement. However, in the frequency range most popular for material characterization (10–100 MHz), the acousto-optical interaction normally results in a multiple-order diffraction pattern symmetrical about the zero-order maximum (Raman–Nath mode). When the nonlinear distortion of the finite-amplitude acoustic wave is taken into account, the asymmetry of the diffraction pattern appears, which is a measure of the material nonlinearity. The theory developed for liquids [155] and solids [156] relates the optical measurements of the diffraction pattern to the acoustic harmonic amplitudes and the distorted wave form. Numerous experiments used the optical detection method in various materials to determine the B/A ratio and the form of the nonlinearly distorted acoustic wave in liquids [17], and the higher harmonic amplitudes and the third-order elastic constants in transparent solids [18,154,157].

The optical detection method can be extended to the nontransparent materials by using SAWs. In particular, the simple optical diffraction pattern for a SAW corresponds to the reflection mode of the diffraction. In this case, the material photoelasticity is not involved and the absolute value of the SAW vertical displacement can be determined by the relative measurements of the intensities for the zero- and first-order diffraction peaks. For intense SAW, the diffraction pattern is also rather straightforward, the intensity of the mth-order diffraction is proportional to the acoustic power of the mth harmonic. For this reason, the absolute amplitudes of the higher SAW harmonics are easily determined by the relative optical measurements [158].

To improve the sensitivity of the optical probing of surface vibrations, the heterodyne laser interferometric techniques have been developed, and the detection of the second-harmonic amplitude smaller than 0.05 A has been demonstrated [19]. In addition to providing the absolute values of the displacement, wide dynamic range, and broadband frequency response the optical methods are noncontact. Recently, an experimental comparison between the capacitive, piezoelectric, and optical detection methods was conducted by Hurley et al. [159]. It was demonstrated that the nonlinear parameters obtained using these three methods were in a good agreement. However, the complexity of the optical systems is still an obstacle for wider practical application of the optical method in the field of nonlinear acoustic NDE.

In contrast to the optical probing systems, the electrodynamic transducer features simplicity and can be used in practical situations. It consists of a metal electrode (of length l) deposited on the face of the sample embedded in an external magnetic field (of induction $\overline{B}$). The mechanical vibrations of the

electrode under the action of an acoustic wave result in the electric voltage appearance across its ends

$$E = ulB \sin \Phi \tag{51}$$

where Φ is the angle between $\overline{B}$ and the particle velocity $G\overline{u}$ on the sample surface. Equation (51) shows that the absolute amplitude of particle velocity (u) can be obtained directly from the measurements of the voltage amplitude. Equation (51) is also applicable to the finite amplitude case: for bulk waves incident on the sample face, the method provides intrinsically broadband detection and according to (51) the output voltage E as a function of time restores the nonlinear wave form of u. In an experiment [122], the electrodynamic transducer was shown to detect higher acoustic harmonics (up to the fourth-order of amplitude $\cong$0.05 A) in a glass sample and to record the nonlinearly distorted wave form.

For the SAW nonlinear experiment the electrode of the transducer is deposited on the substrate surface parallel to the wave front. To provide the broadband operation its width should be small compared with the wavelength of the highest harmonic to be detected. Such a transducer has been used to measure the higher SAW harmonics in $LiNbO_3$ [160] and to reveal the finite-amplitude SAW wave-front distortion in isotropic solids [161].

Accelerometers have also been used for the detection of nonlinearly induced harmonics when relatively low-frequency vibrations (from several hundreds Hz to several kHz) are employed in the resonance or modulation techniques [32]. A vibration-testing machine is normally used to excite the acoustic vibrations at the driving frequency close to one of the natural frequencies of the sample. The accelerometer is mounted on the surface of the sample to record the higher harmonics produced by the resonant nonlinear vibrations. Preliminary calibration of the piezoelectric accelerometers is required to implement the absolute measurements. This method is useful for the nonlinear characterization of relatively large samples, structures, and industrial products.

In summary, the capacitive, optical, piezoelectric, and electrodynamic methods are the four commonly used techniques for the detection of nonlinearly generated ultrasound harmonics. The capacitive detector can provide the highest sensitivity, however it requires the most critical preparation of samples and arrangement of the capacitor. This method is suitable for laboratory use where high precision is the first consideration [15]. The optical method provides many attractive characteristics such as noncontact and broadband operation, a wide dynamic range, and a small testing area. However, its optical system is not compact enough for practical application, and it is used mostly in a laboratory at the present time [19]. This situation is changing because of the introduction of some new techniques, such as using an optical fiber detector [104]. In contrast to the optical probing system, the electrodynamic method features simplicity and can be used in practical situations. It enables us to make direct absolute measurements of the particle velocity and is the intrinsically broadband technique providing the most obvious observation of nonlinear wave distortion effects. The frequency response of a conventional resonant piezoelectric transducer is usually not wide enough for simultaneous study of the multiharmonic wave forms. Use of the broadband mode of the piezoelectric detector is also possible at the expense of sensitivity degradation. The medium sensitivity of the transducer is not an obstacle for nonlinear acoustic-wave detection in materials, which have a high nonlinearity and cause substantial distortion of acoustic waves. Piezoelectric detection will still be an important method in the new practical applications of nonlinear acoustics in the field of NDE.

5. Nonlinear acoustic imaging

In terms of acoustic imaging an obvious implication of the higher harmonic generation in the nonlinear medium is an improvement of an image resolution for a focused acoustic beam configuration. Another important conclusion from the results presented above is that the contrast of the nonlinear acoustic image is determined by local material nonlinearity and can be substantially enhanced in the presence of microinhomogeneous defects. In this section, the effect of these two factors on the operational capability of

acoustic-imaging instruments, and primarily on the acoustic microscope, will be considered. A high local nonlinearity of micro-inhomogeneities can be used for parametric acoustic modulation of the material properties (by a pump wave) in the defected areas "read" by another acoustic wave. Some new opportunities for the nonlinear material characterization using such parametric acoustic imaging will be also discussed.

5.1. Improvement of imaging resolution using higher harmonics

Since the spatial resolution attainable with ultrasound detection equipment is dependent ultimately upon the wavelength of the ultrasound used, the chosen frequency of operation should be high if the size of the object under study is small. However, the higher frequencies attenuate more rapidly in most of the media, particularly in composites and biological tissues, meaning that the depth of the penetration inside the object is reduced as the wavelength of the acoustic field decreases. In practice, a compromise must be established between these two conflicting effects by choosing a transducer of suitable center frequency [27]. One possible method of enhancing the quality of ultrasound images is to exploit the effect of nonlinear propagation on the acoustic signal. The higher harmonic signals generated as it travels through the media can be used to enhance the capability of the traditional ultrasound method.

The possibility of resolution improvement using nonlinearly generated higher harmonics has long been found in the acoustic microscopy. Kompfner and Lemons in 1976 [38] were first to demonstrate second-harmonic imaging in water using a specially tuned acoustic microscope operating at fundamental frequency of 400 MHz. The acoustic microscope was operated in the transmission mode as shown in Fig. 3*a*. The power applied to the transmitter was increased above its normal linear level and the improvement in both the resolution and the contrast of the second-harmonic image compared to the fundamental wave was observed. One of the most striking and in some ways puzzling features of the second-harmonic image was a sharp change in contrast at the boundaries between the various structures of the specimen. This research was furthered by Wickramasinghe and Yeack [162] and similar results were obtained. In both papers, it is pointed out that the second-harmonic signal was generated in the water between the sample and the output lens, but not within the sample itself. This means no nonlinear contribution of the specimen was represented in the acoustic images obtained.

Hadimioglu and Quate [163], and Rugar [148] looked at the problem from a slightly different standpoint. A single transducer and lens were used in their studies, and the acoustic microscope operated in the reflection mode as shown in Fig. 3*b*. For a 4.4 GHz transducer, a resolution of 0.20 m was achieved beyond the theoretical limitation of 0.24 m by increasing the input power [163]. They found that some details in the specimen became visible during the increase of the input power level due to the nonlinear generation of higher harmonics, and the resolution could not be improved further after a certain level of input power was reached. Using a lower frequency (2.0 $\sim$ 2.8 GHz), Rugar [148] found the spatial frequency response of the images formed at nonlinear drive levels to be a factor of 1.4 better than that for conventional linear imaging. The fine details of the sample image contained in the higher harmonics were received by the fundamental-frequency transducer. Rugar claimed that it was attributable to a conversion of the energy in the higher harmonics down to the fundamental frequency in the region behind the object. A theoretical analysis by using the KZK equation was proposed to explain his experimental results. Besides water, liquid nitrogen, and liquid argon were used as coupling media in the study of the nonlinear effects in acoustic microscope [148]. The lower sound velocity, higher nonlinearity, and lower acoustic attenuation in cryogenic fluids make the acoustic nonlinear effects more easily observed [36,39].

By using the acoustic microscope operated at 15.3 GHz and the superfluid 4He with the temperature lower than 0.9 K pressurized to greater than 20 bar as a coupling medium, Moulthrop et al. [36] demonstrated a nearly complete pump depletion at certain input power levels and a reconversion to the pump frequency at higher power levels. When the input level was adjusted to the depletion region, the resolution was improved; on the other hand, when it was adjusted to the reconversion region,

Fig. 3. (*a*)–(*d*) Experimental configurations for improvement of image resolution using higher harmonics.

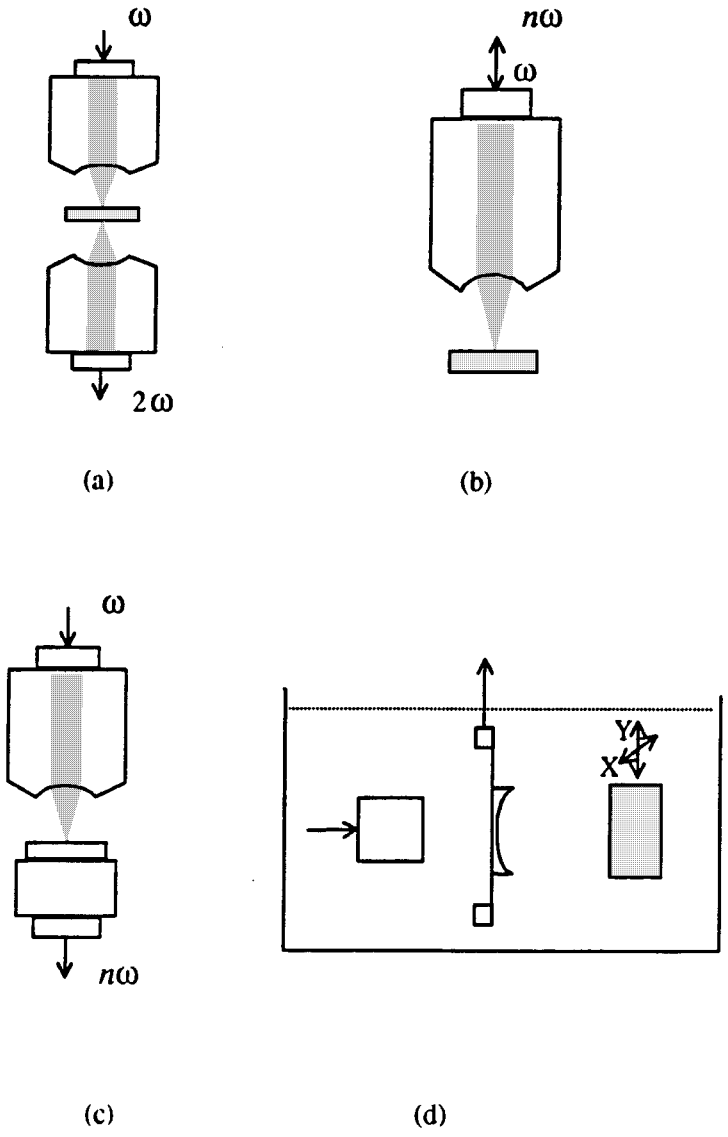

the resolution was obviously degraded. Arguments were presented that the process underlying this nonlinear behavior was associated with harmonic generation. This assumption was verified by Karaki et al. [164,165] using a 370 MHz acoustic microscope operating in the pressurized superfluid 4He at 0.3 K in both reflection and transmission modes with a flat detector, as shown in Fig. 3*c*. The improvement in the resolution for the second harmonic was found to be better by a factor of $2^{1/2}$, possibly due to the special nonlinear properties of the coupling liquid. The nonlinear power dependence of the reflected fundamental wave was similar to that observed by Moulthrop et al. [36].

Germain and Cheeke [39] studied the higher order harmonics using a scanning acoustic microscope operating at a low frequency of 15 MHz with ethanol as the coupling liquid to maximize the higher

harmonic generation. The experimental set-up was similar to that shown in Fig. 3*c*. Despite the frequency used was much lower when compared to those in the investigations introduced above, the detection of the 14th harmonic was achieved. The harmonic components were separated and an improvement in resolution proportional to $n^{1/2}$ for $n \leq 10$ was observed, n being the harmonic number. By using the 10th harmonic, a nonlinear resolution improvement of a factor of 3 was obtained.

The idea that commercial diagnostic B-mode scanners might produce signals with large enough amplitude to cause the appreciable nonlinear effects in normal clinical use was first proposed in 1980 by Muir, Carstensen, and co-workers [166,167]. Later, Starritt et al. [168] demonstrated the nonlinear ultrasound wave distortion in human calf muscle in vivo and in excised bovine liver in vitro using the commercial ultrasound systems. Recently, directed at the improvement of resolution in diagnostic medical ultrasound, Ward et al. [27] investigated nonlinear acoustic imaging in more detail by using a broadband reflection imaging system in water associated with a wire phantom. Their experimental set-up is simplified in Fig. 3*d*. The fundamental frequency employed was 2.25 MHz, and the harmonics up to the fourth order were received and analyzed. Two main types of resolution improvement accompanying the transition from the fundamental frequency to the higher harmonics were noted:

(1) the reflected beamwidth w_n of the wires at the focus decreased according to the relationship $w_n/w_1 = 1/n^{0.78}$ and

(2) the levels of the "sidelobes" in the reflected beams decreased as n went from 1 to 4, n being the harmonic number.

In terms of imaging, these two effects correspond to an enhancement of the lateral resolution of the system and a reduction in the signal-to-clutter ratio. The third type of improvement was due to the gradual decrease in length of the reflected B-mode pulse echoes with increasing n. It was equivalent to a modest enhancement of the axial resolution of the system. Imaging using a combination of harmonics, such as a simple geometrical average, has also been tried for resolution improvement.

Some theoretical work has been done on this subject, predicting an increase of the resolution accompanying the growth of the harmonic number. The theory of converging Gaussian beams predicts that the width of the focal spot for the second harmonic will be $1/2^{1/2}$ times smaller than that for the fundamental wave [148]. Du and Breazeale [169] generalized this result for the case of a Gaussian plane wave, where they found that the spreading of the beam decreased as $1/n^{1/2}$ for the nth harmonic. Their calculations were then applied to the case of a plane Gaussian wave focused by a spherical lens [170].

In summary, the feasibility of nonlinear acoustics use for resolution improvement in ultrasound imaging in both acoustic microscopy and biomedical imaging, has been demonstrated in the literature. Current medical systems do not make significant use of the nonlinearly generated higher harmonics because of (1) the limited response of the receiving transducer at the harmonic frequencies and (2) the limited harmonic levels due to the limitation of the driving power for the safety issue. The first obstacle can be overcome by redesigning the imaging system and by using a broadband transducer, and the second one can be solved by using the microbubble contrast agents [171]. The intravenous injection of microbubbles can greatly enhance the generation of the higher harmonics as well as subharmonics in blood and soft tissues. In acoustic microscopy applications, there is no limitation to the driving power from a safety consideration and so the driving level can be selected for inducing maximum harmonic signals. The imaging resolution can be improved even in the traditional reflection-mode acoustic microscope by operating in the nonlinear region. In addition, coupling media with high nonlinearity, such as cryogenic fluids, can be used to enhance the harmonic generation. The nonlinear effects in the acoustic microscope provide an alternative way to enhance the imaging quality as does an increase in the operation frequency. However, it should be realized that such improvements were obtained because of acoustic nonlinear effects in the coupling liquids or contrast agents, and the nonlinear properties of the tested media were not involved.

Fig. 4. (*a*)–(*c*) Schemes for parametric imaging of acoustic nonlinearity.

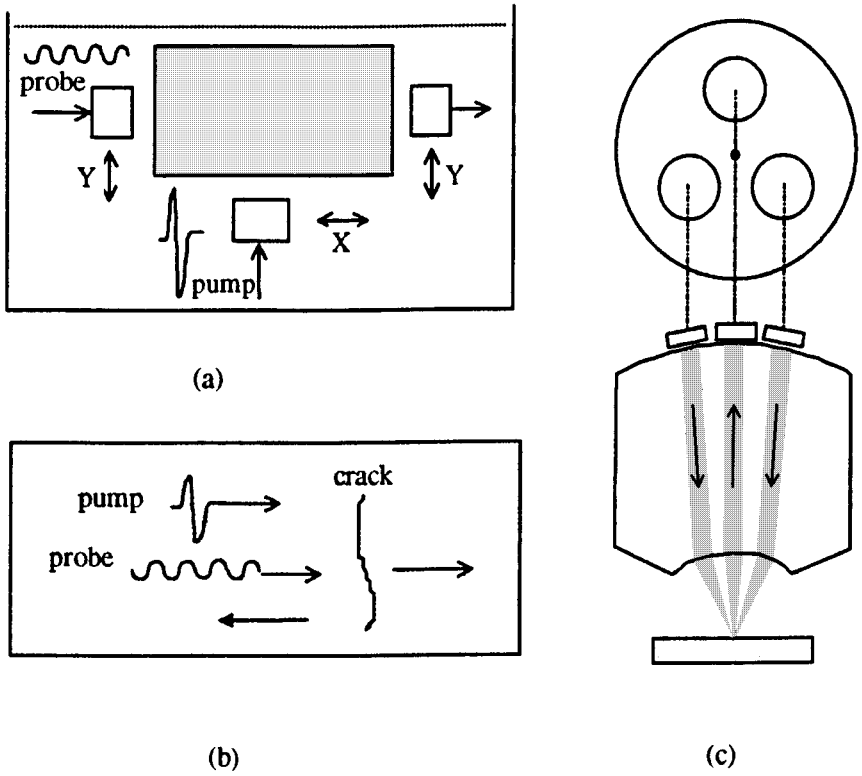

5.2. Parametric imaging of acoustic nonlinearity

Most of the current acoustic imaging systems provide the image of the reflection or transmission coefficient of the media, which is related to some linear material parameter of the sample. As shown in Sect. 3, the nonlinear interaction of acoustic waves can be used to determine the local nonlinear parameter of a specific area in a sample. This provides an opportunity for the imaging of nonlinear properties of the media in biomedical engineering, nondestructive evaluation, and acoustic microscopy.

Nonlinear parametric imaging related to a biomedical application with a frequency lower than 5 MHz was first reported by Ichida et al. [172], their basic idea is shown in Fig. 4*a*. A low-frequency pump wave propagates perpendicularly to a high-frequency (and lower power) continuous probe wave, which is transmitted from one side and received at the opposite side of the sample. The pump frequency is changed to generate a set of cumulative phase shifts of the probe wave; its inverse Fourier transform is proportional to the profile of the nonlinear parameter B/A along the probe-wave propagation path. The nonlinearly (parametrically) modulated probe wave is detected and demodulated to derive the distribution of the B/A along the probe-wave propagation path. This technique was later modified by the use of impulsive pump wave forms allowing for the generation of real-time transmission-mode nonlinear parametric imaging [173], and with the pump wave applied from the opposite direction to the probe wave for practical applications [174]. Cain [175] also derived a theoretical expression for the phase shift in a sinusoidal probe wave due to nonlinear interaction with an arbitrary pump wave propagating in the opposite direction.

Recently, this nonlinear imaging technique has been further improved to operate in the reflection mode considering the application in human body, where one side access is always more practical

[176]. Nakagawa et al. [177] have proposed a somewhat different method to construct a nonlinear type of ultrasonic system based on the nonlinear interaction resulting in the generation of the sum and difference frequency waves. The amplitude of the received wave with the difference frequency depends on the attenuation and nonlinear parameter of media, so the tomographic image of the nonlinear parameter can be reconstructed with the compensation by the results of the conventional (attenuation) tomography. The quality of the images obtained in these studies was not good enough for clinical purpose and the biological effects of the high-power pump waves should be further studied. However, this technique provides a new opportunity for parametric imaging of human body, in which more complete characterization of biological tissues is desired beyond the capability of the conventional B-mode backscatter imaging.

The feasibility of using a similar method for the nonlinear tomography in seismology has also been discussed [32]. In addition, an NDE analog for detecting and locating cracks in materials has been proposed, as shown in Fig. 4*b* [32]. The stress in a high-power pump pulse alters the crack opening and parametrically changes the phase and amplitude of the transmitting or reflecting probe wave. By measuring the phase or amplitude modulation of the wave received, one can detect the crack presence and its location. The pump wave can be induced from the same side as the probe wave, or from the opposite side of the sample. A similar tomography scheme, which uses oppositely directed SAWs and a nonlinearly generated double-frequency output signal, was discussed in Sect. 3 and 4, and applied to nonlinear NDE of the surface-fracture defects [31]. This obviously demonstrates the potential for prospective applications of nonlinear NDE; however, more investigations in this area are required for the nonlinear acoustic approach to be accepted in industry and technology.

In the acoustic microscopy application, the parametric nonlinear interaction of two acoustic beams formed by two lenses was first proposed by Kompfner and Lemons [38] and Wickramasinghe and Yeack [162]; then it was used to obtain nonlinear imaging of some samples by Tan et al. [178], and Ransom et al. [40]. Figure 4*c* shows the experimental configuration for a nonlinear acoustic microscope [179], in which two transducers with frequencies of 640 MHz (f_1) and 760 MHz (f_2), were used to transmit the ultrasound waves, and the third transducer with frequency of 520 MHz ($2f_1 - f_2$) was used as a receiver. The transducers were mounted on the curved back surface of a fused quartz lens, with the geometry designed so that the transducers were confocal in the water [178]. The nonlinear interaction was adjusted to occur on the surface of the sample, and the nonlinear interaction in the coupling liquid was supposed to be reduced. However, this first attempt has not revealed any nonlinear effects ascribed to the specimen rather than to the water [178]. A similar set-up using four transducers was reported later [40]. These results showed that the regions with different third-order elastic constants in a sample, i.e., different nonlinear properties, can be clearly differentiated by using the nonlinear mode; that difference, however, could not be observed by a traditional acoustic microscope operating in linear mode.

According to Sect. 3.4, the higher nonlinear contrast should be expected for the areas with a strong acoustic nonlinearity (disbonds, cracks, etc.) due to CAN. The nonlinear acoustic microscopy of the CAN area has recently been reported [180]. The second-harmonic image in a 25 MHz acoustic microscope operating in a reflection mode clearly identified the "kissing bond" contour around a weld spot in steel plates. Although not too much research has been carried out in this area, the prospects for the nonlinear imaging in acoustic microscopy have been certainly demonstrated. It can provide additional information on the material properties and micro-inhomegeneities that cannot be obtained by means of conventional (linear) acoustic microscopy.

6. Conclusions and discussion

The nonlinear acoustic approach, systematically established since the 1960s–1970s, has been widely used for the characterization of various materials during the past few decades. There are three nonlinear phenomena accompanying the finite-amplitude acoustic-wave propagation (and reflection) that have been shown to be of practical value for materials technology: the acoustic-wave velocity dependence

on the stress (strain) in the material, higher harmonic generation, and three-wave nonlinear acoustic interactions.

To quantitatively assess the acoustic nonlinearity, the following parameters are usually defined: the nonlinear coefficients β_n of the higher order terms in the local speed variation of an acoustic wave with particle velocity (or strain), nonlinearity parameter B/A representing the normalized coefficient of the quadratic term in the material equation of state, and the acoustoelastic constant, indicating the relation between the acoustic-wave velocity and the stress (strain) applied to a solid material. They all depend solely on the basic linear and nonlinear elastic parameters of the material. The nonlinear coefficients β_n and acoustoelastic constant are usually used for characterization of solid media, while the nonlinearity parameter B/A is widely applied to liquid media and biological soft tissues. The second-order nonlinear coefficients (β_n and B/A) are usually involved in characterizing the elastic nonlinearity for the majority of liquids and flawless solids. In imperfect (nonclassical) solid materials the higher order nonlinear effects could be manifested dramatically and the higher order nonlinear coefficients β_n should also be taken into account.

For various media, acoustic-wave nonlinear behavior is affected by the relation between the nonlinearity, attenuation, dispersion, and diffraction. To evaluate a quantitative contribution of the nonlinear parameters in each particular case, the solutions of the nonlinear Burgers, KDV, and KZK equations are used. On the basis of the relations obtained, the nonlinear coefficients β_2, β_3 can be experimentally determined by the measurements of the second- and third-harmonic generation, which is referred to as the finite-amplitude method. The resonance method for β_2, β_3 determination employs the harmonics generation, standing-wave interaction (modulation) in a solid resonator or a resonant frequency shift as a function of applied stress. The nonlinearity parameter B/A in liquids can also be obtained by the thermodynamic method based on the measurements of the acoustic-velocity dependence on the temperature and pressure. The acoustoelastic constant is determined by measuring the change in the wave velocity as a function of the external load applied to the solid material, this is referred to as the acoustoelastic method. In homogeneous materials the nonlinear coefficient β_2 is generally under 10, however, it can reach 10^4 in inhomogeneous media or materials with specific defects.

For homogeneous (flawless) solids, the acoustic nonlinearity is a direct measure of the lattice anharmonicity, and measurements of β_n (the higher order elastic constants) deliver unique information on the material thermoelastic properties and phonon–gas parameters. The nonlinear elastic properties of solids containing micro- and macro-defects may manifest themselves in specific types of acoustic nonlinearity that can be used as a measure of "defectiveness" of the material or the integrity of a product structure. The experimental acoustic methods for the higher order elastic constants measurements have been demonstrated to be useful for the nondestructive evaluation of various disruptions in solid materials, like dislocations in crystals, fractions of precipitates in metallic alloys, microcracks, disbonds, and other defects.

The experimental nonlinear methods employ various types of finite-amplitude bulk, surface, and interface acoustic waves. The finite-amplitude method works well at high ultrasonic frequencies for the materials with a strong nonlinearity and low acoustic attenuation. The acoustoelastic and resonance techniques are less affected by the attenuation in solids, so they are advantageous for use with imperfect (constructional, defective, etc.) materials. The specificity of the nonlinear acoustic experiments is concerned with "nonreciprocal" detection, combined with high sensitivity, and absolute-amplitude measurements. The comparative analysis of the most commonly used detection methods (capacitive, piezoelectric, optical, electrodynamic, and accelerometric) showed that at present the piezoelectric detector is still the most adequate for many of nonlinear acoustic applications.

Experimental investigations unambiguously proved a strong correlation between the material nonlinear coefficients and the growth of defects in the materials, i.e., their strength degradation. Therefore, the measurements of β_n provide unique information on the material strength and can be used to predict its failure far in advance. The reason for such a correlation is associated with acoustic nonlinear

phenomena on the internal contact interfaces separating the intact material and the inclusions (cracks, grains, disbonds, etc.). Even a weakly nonlinear acoustic wave incident on the ideally bonded (or free) contact interface, causes an efficient reflected and transmitted higher harmonic generation. The partially clamped contact interface demonstrates an anomalously high nonlinearity (CAN) connected with clapping of the contact faces and accompanied by not only superharmonic but also subharmonic generation, and chaotic dynamics. An alternative efficient mechanism of CAN for rough contacts is concerned with the Hertzian nonlinearity. The values of β_n measured for CAN are orders of magnitude higher than those for homogeneous materials. Another feature of CAN is related to an abnormally efficient third-harmonic generation and non-monotonic spectral distribution of the higher harmonics.

Due to high β_n values, the CAN areas (and, therefore, partially closed cracks) represent an abrupt nonlinear inhomogeneity for an incident acoustic wave. It stipulates an efficient higher backward harmonic generation (nonlinear reflection). The efficiency of nonlinear reflection for the higher harmonics from such cracks is about two to three orders of magnitude higher than that for the linear reflection. This clearly shows the advisability of the nonlinear reflection mode in NDE of the cracked inclusions and disbonds "invisible" with conventional acoustic instruments.

In terms of acoustic imaging, an obvious implication of the higher harmonic generation in a nonlinear medium is an improvement of image resolution for a focused acoustic beam configuration. This research has been greatly enhanced by the introduction of intravenous-injected contract agents such as microbubbles in the biomedical imaging. Similar to the cracked defects, nonlinear bubble dynamics makes the coupling agent extremely nonlinear. The second category of investigations is focused on the imaging of material nonlinear parameters. These two analogous areas of investigations have been conducted in the acoustic microscopy configurations in the frequency range from 500 MHz to 15 GHz. An obvious improvement of the image resolution has been obtained by increasing the driving power of the transducer to make the acoustic microscope operate in the nonlinear region.

To obtain the mapping of the sample's nonlinear properties, a three-wave interaction mode of acoustic microscopy has been developed. It uses the amplitude of the mixed frequency signal, resulting from nonlinear interaction between two focused beams, as an indicator of local material nonlinearity strength. For a strong local nonlinearity (like CAN), second-harmonic focused beam acoustic microscopy can also be used. An alternative plane-wave configuration is a parametric acoustic imaging system applied in biomedical research, seismology, and NDE. In the latter case, a high local nonlinearity of micro-inhomogeneities is used for parametric acoustic modulation (by a pump wave) of the material properties in the defected areas which is "read" by another (probing) acoustic wave. Both the surface and bulk acoustic-wave parametric configurations have been tested in experiment, and have demonstrated new opportunities for tomographic nonlinear acoustic imaging.

The present review also indicates some urgent issues for further investigation. New theoretical approaches are required to quantify adequately some nonclassical types of elastic nonlinearity observed in inhomogeneous materials. Unlike optics [1], acoustic-wave reflection and transmission (especially in solids) have long been considered as linear phenomena. The experimental and theoretical data obtained in nonlinear acoustics of solids over the last decade demonstrate the need to develop the nonlinear acoustic approach to their analysis. A comprehensive research of the finite-amplitude acoustic-wave propagation through (and reflection from) the nonlinear interfaces is crucial for further development of nonlinear diagnostics of inhomogeneous materials.

Acoustic nonlinear contact phenomena are important practically for a wide range of nonlinear applications in material technology. Several unusual aspects of CAN demonstrated in experiment (subharmonics, nonlinear chaos, non-monotone harmonic spectral distribution, etc.) are to be supplemented with a thorough experimental study and theoretical analysis that would substantiate their application area in the nonlinear material characterization.

The nonlinear acoustics imaging investigations were mostly focused in two frequency ranges: higher than 500 MHz based on the high-resolution acoustic microscopy technique and lower than 20 MHz

for biomedical imaging. However, the nonlinear effects in acoustic microscopy of medium frequencies, i.e., from 20 to 100 MHz have not yet been well investigated. Medium-frequency range microscopy has been demonstrated to be very useful in the evaluation of various materials and imperfections, such as spot welding [181]; biological tissue [182]; composites, crystals, and metallic samples [183]. Besides providing medium resolution, it is easy to operate and maintain with low cost, which are important factors for an extensive industrial application. On the other hand, this review demonstrates that acoustical nonlinearity in this frequency range is manifested dramatically, particularly, at the level of microdefects. Therefore, the nonlinear mode of medium-range microscopy would enhance its capability for the material characterization and imaging of cracked micro-inhomogeneities crucial for integrity of high-damage risk materials and products used in aviation technology, nuclear-power engineering, and microelectronics.

On the basis of the results presented in this review, we can conclude that the scientific research implemented so far has resulted in a deeper understanding of the physics involved in nonlinear elasticity and demonstrated the obvious potential of nonlinear acoustics in material characterization. In a practical context, more investigations are required to provide additional information about the nonlinear properties of various defects in materials widely used in industry and technology. Direct comparison between the capabilities of linear and nonlinear acoustic techniques in a number of practical situations can assist the new nonlinear NDE philosophy to be considered as a serious complement to its mature linear counterpart. In addition, instrumentation manufacturers should provide more experimental apparatus and electronic components suitable for nonlinear acoustic research and applications. Thus, further development and promotion of the nonlinear acoustic techniques in materials technology and NDE requires the cooperation of universities (ideas and research), industry (initiation of applications and funds), and instrumentation manufacturers (equipment and components).

References

1. N. Bloembergen. Nonlinear optics. World Scientific, Singapore. 1996.
2. M.F. Hamilton and D.T. Blackstock (*editors*). Nonlinear acoustics. Academic Press, San Diego. 1997.
3. R.T. Beyer. Nonlinear acoustics in fluids. Benchmark papers in acoustics. Vol. 18. Nostrand Reinhold Co., New York. 1984.
4. P.J. Westervelt. J. Acoust. Soc. Am. **32**, 934 (1960).
5. R.T. Beyer. J. Acoust. Soc. Am. **32**, 719 (1960).
6. P.J. Westervelt. J. Acoust. Soc. Am. **35**, 535 (1963).
7. M.F. Hamilton. Nonlinear wave propagation in Mechanics. AMD (Symposia Series), Applied Mechanics Division, American Society of Mechanical Engineers. **77**, 1 (1986).
8. L.K. Zarembo and V.A. Krasilnikov. Introduction to nonlinear acoustics. Nauka, Moscow, 1966.
9. B.K. Novikov, O.V. Rudenko, and V.I. Timoshenko. Nonlinear underwater acoustics, Sudostroenie, Leningrad. 1981.
10. R.T. Beyer. *In* Physical acoustics: Principles and methods IIB. *Edited by* W.P. Mason. Academic Press, New York. 1965.
11. R.T. Beyer. Nonlinear acoustics. Naval Sea System command, Washington DC. 1974.
12. O.V. Rudenko and S.I. Soluyan. Theoretical foundations of nonlinear acoustics. Consultants Bureau, New York. 1977.
13. N.S. Bakhvalov, Ya.M. Zhileikin, and E.A. Zabolotskaya. Nonlinear theory of sound beams. Nauka, Moscow. 1982.
14. L.K. Zarembo and V.I. Timoshenko. Nonlinear acoustics. Moscow University, 1984.
15. M.A. Breazeale and J. Philip. *In* Physical acoustics. Vol. XVII. *Edited by* W.P. Mason. Academic Press, New York. 1980. pp. 1-60.
16. J.H. Cantrell and W.T. Yost. Philos. Mag. **A69**, 315 (1994).
17. L.E. Hargrove and K. Achiuthan. *In* Physical acoustics. Vol. II B. *Edited by* W.P. Mason. Academic Press, New York. 1965.
18. D.H. McMagon. J. Acoust. Soc. Am. **45,** 1007 (1968).

19. A. Moreau. J. Acoust. Soc. Am. **98**, 2745 (1995).
20. I.E. Dekalo, V.V. Palachev, O.Yu. Serdobol'skaya, S.P. Tokmakova, I.A. Chaban, and V.P. Shabatin. Russian ultrasonics. **23**, 333 (1993).
21. G.D. Meegan, Jr., P.A. Johnson, R.A. Guyer, and K.R. McCall. J. Acoust. Soc. Am. **94**, 3387 (1993).
22. R.A. Guyer, K.R. McCall, and K.E.A. Van Den Abeele. Geophys. Res. Lett. **25**, 1585 (1998).
23. E.H. Field, P.A. Johnson, I.A. Beresnev, and Y. Zheng. Nature, **390**, 599 (1997).
24. R.A. Guyer and P.A. Johnson. Physics Today, **52**, 30 (1999).
25. R. Beyer. *In* Nonlinear acoustics. *Edited by* M.F. Hamilton and D.T. Blackstock. Academic Press. San Diego. U.S.A. 1997. p. 25.
26. E.L. Carstensen and D.R. Bacon. *In* Nonlinear acoustics. *Edited by* M.F. Hamilton and D.T. Blackstock. Academic Press. San Diego. U.S.A. 1997. p. 421.
27. B. Ward, A.C. Baker, and V.F. Humphrey. J. Acoust. Soc. Am. **101**, 143 (1997).
28. N. Ichida, T. Sato, and M. Linzer. Ultrasonic Imaging, **5**, 295 (1983).
29. J.H. Cantrell and W.T. Yost. J. Appl. Phys. **81**, 2957 (1997).
30. S.U. Fassbender, M. Kroening, and W. Arnold. Mater. Sci. Forum, (Part 2, Nondestructive characterization of materials VII), **210**, 783 (1996).
31. I.Yu. Solodov. Ultrasonics, **36**, 383 (1998).
32. A.M. Sutin and V.E. Nazarov. Radiophys. Quantum Electron. **38**, 109 (1995).
33. A.M. Sutin, C. Delclos, and M. Lenclud. *In* Proc. 2nd Int. Symp. on Acoustic and Vibration Surveillance Methods and Diagnostic Techniques. Senlis, France. 1995. p. 725.
34. L.K. Zarembo, V.A. Krasil'nikov, and I.E. Shkol'nik. Soviet J. Nondestructive Testing. **25**, 706 (1990).
35. J.K. Na, W.T. Yost, and J.H.Cantrell. *In* Review of Progress in Quantitative Nondestructive Evaluation. Vol. 12B. *Edited by* D.O. Thompson and D.E. Chimenti. Plenum Press, New York. 1993. p. 2075.
36. A.A. Moulthrop, M.S. Muha, G.C. Kozlowski, and C.P. Silva. *In* Proc. 1990 Ultrasonics Symp. p. 907.
37. K.E.A. Van Den Abeele, J. Carmeliet, J.A. TenCate, and P.A. Johnson. *In* Proc. 2nd. Int. Conf. Emerging Technologies in NDT. Athens, 1999. (In press).
38. R. Kompfner and R.A. Lemons. Appl. Phys. Lett. **28**, 295 (1976).
39. L. Germain and J.D.N. Cheeke. J. Acoust. Soc. Am. **83**, 942 (1988).
40. H.L. Ransom, Jr., S.W. Meeks, and C.C. Cutler. *In* Proc. 1986 Ultrasonic Symp. p. 731.
41. D.T. Blackstock. *In* American Institute of Physics handbook. 3rd. ed. *Edited by* D.E. Gray. McGraw, New York. 1972.
42. R.N. Thurston and M.J. Shapiro. J. Acoust. Soc. Am. **41**, 1112 (1967).
43. M.F. Hamilton and D.T. Blackstock. J. Acoust. Soc. Am. **83**, 74 (1983).
44. V.A. Krasilnikov and V.V. Krylov. Introduction to physical acoustics. Nauka, Moscow. 1984.
45. B.A. Konyukhov and G.M. Shalashov. Appl. Math. Phys. **23**, 125 (1974).
46. M.A. Breazeale and J. Ford. J. Acoust. Soc. Am. **36**, 3486 (1965).
47. T. Bateman, M.P. Mason, and H.J. McSkimin. J. Appl. Phys. **32**, 928 (1961).
48. J.H. Cantrell and K. Salama. Int. Mater. Rev. **36**, 125 (1991).
49. M.B. Vinogradova, O.V. Rudenko, and A.P. Sukhorukov. Wave theory. Nauka, Moscow. 1990.
50. E.A. Zabolotskaya and R.V. Khokhlov. Sov. Phys. Acoust. **15**, 35 (1969).
51. V.P. Kuznetsov. Sov. Phys. Acoust. **16**, 467 (1970).
52. N.J. Tjotta and S. Tjotta. J. Acoust. Soc. Am. **69**, 1644 (1981).
53. G.S. Garrett, N.J. Tjotta, and S. Tjotta. J. Acoust. Soc. Am. **74**, 1013 (1983).
54. S.I. Aanonsen, T. Barkve, N.J. Tjotta, and S. Tjotta. J. Acoust. Soc. Am. **75**, 749 (1984).
55. M.F. Hamilton, N.J. Tjotta, and S. Tjotta. J. Acoust. Soc. Am. **78**, 202 (1985).
56. A.J. Watson, V.F. Humphrey, A.C. Baker, and F.A. Duck. *In* Frontiers of nonlinear acoustics: 12th ISNA. *Edited by* M.F. Hamilton and D.T. Blackstock. Elsevier Science, London. 1990. p. 445.
57. A.C. Baker. J. Acoust. Soc. Am. **91**, 713 (1992).
58. A.C. Baker, A.M. Berg, A. Sahin, and N.J. Tjotta. J. Acoust. Soc. Am. **97**, 3510 (1995).
59. A.C. Baker, B. Ward, and V.F. Humphrey. J. Acoust. Soc. Am. **100**, 2062 (1996).
60. M.F. Hamilton, N.J. Tjotta, and S. Tjotta. J. Acoust. Soc. Am. **82**, 311 (1987).
61. N.J. Tjotta and S. Tjotta. J. Acoust. Soc. Am. **83**, 487 (1988).
62. C.M. Darvennes and M.F. Hamilton. J. Acoust. Soc. Am. **87**, 1955 (1990).
63. C.M. Darvennes, M.F. Hamilton, N.J. Tjotta, and S. Tjotta. J. Acoust. Soc. Am. **89**, 1028 (1991).

64. D.J. Holcomb. J. Geophys. Res. **86**, 6235 (1981).
65. G.N. Boinott. Los Alamos Nat. Lab. Rep. **LA-UR-93-3839**, 121 (1993).
66. K.R. McCall and R.A. Guyer. J. Geophys. Res. **99**, 23 887 (1994).
67. F. Preisach. Z. Phys. **94**, 277 (1935).
68. I.D. Mayergoyz. J. Appl. Phys. **57**, 3803 (1985).
69. K.R. McCall and R.A. Guyer. Nonlinear Proc. Geophys. **3**, 89 (1996).
70. R.A. Guyer, K.R. McCall, and G.N. Boinott. Phys. Rev. Lett. **74**, 3491 (1995).
71. K.E.A. Van Den Abeele, P.A. Johnson, R.A. Guyer, and K.R. McCall. J. Acoust. Soc. Am. **101**, 1885 (1997).
72. R. Truell, C. Elbaum, and B.B. Chick. Ultrasonic methods in solid state physics. Academic, New York. 1969.
73. D.S. Hughes and J.L. Kelly. Phys. Rev. **92**, 1145 (1953).
74. R.R. Rao and A. Ramanand. Phys. Status Solidi, **58A**, 11 (1980).
75. E.P. Papadakis. *In* Physical acoustics. Vol. 17. *Edited by* W.P. Mason and R.N. Thurston. Academic Press, New York. 1976. p. 277.
76. M.A. Breazeale, J.H. Cantrell, and J.S. Heyman. *In* Methods of experimental physics. Vol. 19. *Edited by* F.D. Edmonds. Academic Press, New York. 1981. p. 67.
77. J.S. Heyman, S.G. Allison, K. Salama, and S.I. Chu. *In* Proc. Symp. NDE Appl. Mater. Process. American Society for Metals, Metals Park, Ohio. 1983. p. 177.
78. S.G. Allison, J.S. Heyman, and K. Salama. *In* Proc. IEEE Ultrasonics Symp. IEEE, New York. 1984. p. 997.
79. E. Schneider, S.K. Chu, and K. Salama. *In* Proc. IEEE Ultrasonics Symp. IEEE, New York. 1984. p. 944.
80. S. Razvi, P. Li, K. Salama, J.H. Cantrell, and W.T. Yost. *In* Review of progress in quantitative nondestructive evaluation. Vol. 6B. *Edited by* D.O. Thompson and D.E. Chimenti. Plenum Press, New York. 1987. p. 1403.
81. B. Grelsson and K. Salama. *In* Review of progress in quantitative nondestructive evaluation. Vol. 9B. *Edited by* D.O. Thompson and D.E. Chimenti. Plenum Press, New York. 1989. p. 1441.
82. O. Buck, L.A. Ahlberg, L.J. Graham, G.A. Alers, C.A. Wert, and K.C. Hsieh. Phys. Status Solidi, **55A**, 223 (1979).
83. K. Salama and C.K. Ling. J. Appl. Phys. **51**, 1505 (1980).
84. M. Namkung, D. Utrata, S.G. Allison, and J.S. Heyman. *In* Review of progress in quantitative nondestructive evaluation Vol. 5B. *Edited by* D.O. Thompson and D.E. Chimenti. Plenum Press, New York. 1985. p. 1481.
85. P. Nagy. Ultrasonics, **36**, 375 (1998).
86. G.S. Kino, D.M. Barnett, N. Grayeli, G. Herrmann, J.B. Hunter, D.B. Ilie, G.C. Johnson, R.B. King, M.P. Scott, J.C. Shyne, and C.R. Steele. J. Nondestruct. Eval. **1**, 67 (1980).
87. G.E. Dace, O. Buck, and R.B. Thompson. *In* Vibro-acoustic characterization of materials and structures. Vol. 14. ASME, NCA, New York. 1992. p. 221.
88. A.A. Gedroitz and V.A. Krasilnikov. Sov. Phys. JETP, **16**, 1122 (1963).
89. M.A. Breazeale and D.O. Thompson. Appl. Phys. Lett. **3**, 77 (1963).
90. R.D. Peters and M.A. Breazeale. Appl. Phys. Lett. **12**, 106 (1968).
91. R.N. Trebits. Ph.D. thesis. Georgia Institute of Technology, Atlanta. (1972).
92. D. Gerlich and M.A. Breazeale. J. Appl. Phys. **63**, 5712 (1988).
93. V.E. Lyamov. Polarization effects and anisotropy of acoustic waves interaction in crystals. Moscow State University. Moscow. 1983.
94. W.T. Yost, J.H. Cantrell, and M.A. Breazeale. J. Appl. Phys. **51**, 126 (1981).
95. J.K. Na and M.A. Breazeale. J. Acoust. Soc. Am. **95**, 3213 (1994).
96. K. Van Den Abeele and M.A. Breazeale. J. Acoust. Soc. Am. **99**, 1430, (1996).
97. A.A. Gedroitz, L.K. Zarembo, and V.A. Krasilnikov. Dokl. USSR Acad. Sci. **150,** 515 (1963).
98. A. Hikata, B. Chick, and C. Elbaum. Appl. Phys. Lett. **3**, 195 (1963).
99. K.K. Ermilin, L.K. Zarembo, and V.A. Krasilnikov. Phys. Mater. **38**, 880 (1974).
100. J.K. Na, J.H. Cantrell, and W.T. Yost. *In* Review of progress in quantitative nondestructive evaluation. Vol. 15. *Edited by* D.O. Thompson and D.E. Chimenti. Plenum Press, New York. 1996. p. 1347.
101. J.H. Cantrell. J. Appl. Phys. **76**, 3372 (1994).

102. L.A. Ostrovsky. J. Acoust. Soc. Am. **90**, 3332 (1991).
103. J.H. Cantrell, W.T. Yost, S. Razvi, P. Li, and K. Salama. *In* Proc. IEEE Ultrasonics Symp. New York. 1986. p. 1075.
104. J.H. Cantrell and G. Zhang. J. Appl. Phys. **84**, 5469 (1998).
105. F. Birch. Handbook of physical constants. *Edited by* S.P. Clark, Jr. Geol. Soc. Am. Press. Boulder. Colo. 1966. p. 97.
106. G.D. Meegan, Jr., P.A. Johnson, R.A. Guyer, and K.R. McCall. J. Acoust. Soc. Am. **94**, 3387 (1993).
107. K.E.A. Van Den Abeele and P.A.Johnson. J. Acoust. Soc. Am. **99**, 3346 (1996).
108. J.A. TenCate, K.E.A. Van Den Abeele, T.J. Shankland, and P.A. Johnson. J. Acoust. Soc. Am. **100**, 1383 (1996).
109. K.E.A. Van Den Abeele. J. Acoust. Soc. Am. **99**, 3334 (1996).
110. L.K. Zarembo, V.A. Krasilnikov, V.N. Slutch, and O.Yu. Serdobolskaya. Akust. Zh. **12**, 486 (1966).
111. A.S. Korotkov, M.M. Slavinskii, and A.M. Sutin. Akust. Zh. **40**, 84 (1994).
112. A.S. Korotkov and A.M. Sutin. Acoust. Lett. **18**, 59 (1994).
113. R.G. Maev and I.Yu. Solodov. *In* Abstracts review of progress in quantitative nondestructive evaluation. Montreal, Canada. 1999. p. 46.
114. V.E. Nazarov. Akust. Zh. **37**, 150 (1991).
115. P.A. Johnson, B. Zinszner, and P.N.J. Rasolofosaon. J. Geophys. Res. **101**, 11 553 (1996).
116. Y. Shui and I.Yu. Solodov. J. Appl. Phys. **64**, 6155 (1988).
117. I.Yu. Solodov. J. Appl. Phys. **64**, 2901 (1988).
118. S. Zhou, W. Jiang, and Y. Shui. J. Appl. Phys. **78**, 39 (1995).
119. F.M. Severin, I.Yu. Solodov, and B.A. Korshak. Vestnik Moskovskogo Universiteta, **40**, 34 (1999).
120. F.M. Severin, I.Yu. Solodov, and Yu.N. Shkoulanov. Vestnik Moskovskogo Universiteta, **29**, 94 (1988).
121. F.M. Severin. Ph.D. thesis. Moscow State University. Moscow. 1990.
122. K.S. Len, F.M. Severin, and I.Yu. Solodov. Sov. Phys. Acoust. **37**, 610 (1991).
123. I.Yu. Solodov and C. Wu. Acoust. Phys. **39**, 476 (1993).
124. J.M. Richardson. Int. J. Eng. Sci. **17**, 73 (1979).
125. J.D. Achenbach and A.N. Norris. J. Nondestruct. Eval. **3**, 229 (1982).
126. S. Hirose and J.D. Achenbach. J. Acoust. Soc. Am. **93**, 142 (1993).
127. R.B. Thompson, C.J. Fiedler, and O. Buck. *In* Nondestructive methods for material property determination. *Edited by* C.O. Ruud and R.E. Green. Plenum, New York. 1984. p. 161.
128. R.B. Thompson and C.J. Fiedler. *In* Review of progress in quantitative NDE. Vol. 3A. *Edited by* D.O. Thompson and D.E. Chimenti. Plenum, New York. 1984. p. 207.
129. L.D. Landau and I.E. Lifshits. Theory of elasticity. Pergamon. Tarrytown. N.Y. 1986.
130. O.V. Rudenko and C. Wu. Vestnik Moskovskogo Universiteta, **34**, 94 (1993).
131. O. Buck, W.L. Morris, and J.M. Richardson. Appl. Phys. Lett. **33**, 371 (1978).
132. W.L. Morris, O. Buck, and R.V. Inman. J. Appl. Phys. **50**, 6737 (1979).
133. K.S. Len and I.Yu. Solodov. Acoust.Phys. **39,** 149 (1993).
134. I.Yu. Solodov and A.F. Asainov. *In* Non-destructive testing. *Edited by* K.V. Van Hemelrijck and G. Anastassopoulos. Balkema, Rotterdam. 1996. p. 73.
135. R.G. Maev and I.Yu. Solodov. *In* Proc. IEEE Ultrason. Symp. Sendai, Japan. Vol.1. 1998. p. 707.
136. A.F.Asainov, K.S. Len, and I.Yu. Solodov. Acoust.Phys. **39,** 311 (1993).
137. K.S. Len and I.Yu. Solodov. Acad. Sci. DPR Korea. **3**, 29 (1994).
138. D.V. Armyakov, A.F. Asainov, B.A. Korshak, and I.Yu. Solodov. Defektoskopiya, **12**, 34 (1998).
139. W.K. Law, L.A. Frizzell, and F. Dunn. Ultrasound Med. Biol. **11**, 307 (1985).
140. X. Gong, Z. Zhu, T. Shi, and J. Huang. J. Acoust. Soc. Am. **86**, 1 (1989).
141. L. Germain, R. Jacques, and J.D.N. Cheeke. J. Acoust. Soc. Am. **86**, 1560 (1989).
142. P.J. Vella, T.C. Padmore, and G.I. Stegeman. J. Appl. Phys. **45**, 1993 (1974).
143. Y.W. Mao, Y. Shui, W. Jiang, Z. Lu, and W. Wu. Appl. Phys. Lett. **55**, 2394 (1989).
144. A.F. Asainov, K.S. Len, and I.Yu. Solodov. Sov. Phys. Acoust. **38**, 293 (1992).
145. F.M. Severin and I.Yu. Solodov. Vestnik Moskovskogo Universiteta, **29**, 84 (1988).
146. I.Yu. Solodov, A.F. Asainov, and K.S. Len. Ultrasonics, **31**, 91 (1993).
147. P.A. Johnson, A. Migliori, and T.J. Shankland. J. Acoust. Soc. Am. **89**, 598 (1991).
148. D. Rugar. J. Appl. Phys. **56**, 1338 (1984).

149. P. Cervenka and P. Alais. J. Acoust. Soc. Am. **88**, 473 (1990).
150. V.E. Gusev and A.A. Karabutov. Laser acoustics. Nauka, Moscow, 1993.
151. A.C. Baker. Phys. Med. Biol. **36**, 1457 (1991).
152. K.S. Len. Ph.D. thesis. Moscow State University. 1993.
153. X. Jia, A. Boumiz, and G. Quentin. Appl. Phys. Lett. **63**, 2192 (1993).
154. L. Adler, X. Jia, and G. Quentin. Proc. SPIE, **2643**, 228 (1995)
155. B.D. Cook. JASA, **33**, 832 (1961).
156. J. Melngailis, A.A. Maradudin, and A. Seeger. Phys. Rev. **131**, 172 (1963).
157. C.T. Shaun, C.L. Anthony, and G.F. Ian. J. Acoust. Soc. Am. **93**, 148 (1993).
158. I.B. Yakovkin and D.V. Petrov. Light diffraction on surface acoustic waves. Nauka, Novosibirsk. 1979.
159. D.C. Hurley, W.T. Yost, E.S. Boltz, and C.M. Fortunko. *In* Review of progress in quantitative nondestructive evaluation. Vol. 16. *Edited by* D.O. Thompson and D.E. Chimenti. Plenum Press, New York. 1997. p. 1383.
160. A.A. Podgornov. Ph.D. thesis. Moscow State University. 1984.
161. A.P. Brysev, V.A. Krasilnikov, A.A. Podgornov, and I.Yu. Solodov. Fizika Tverdogo Tela. **26**, 2104 (1984).
162. H.K. Wickramasinghe and C. Yeack. J. Appl. Lett. **48**, 4951 (1977).
163. B. Hadimioglu and C.F. Quate. Appl. Phys. Lett. **43**, 1006 (1983).
164. K. Karaki, T. Saito, K. Matsumoto, and Y. Okuda. Physica B, **165**, 131 (1990).
165. K. Karaki, T. Saito, K. Matsumoto, and Y. Okuda. Appl. Phys. Lett. **59**, 909 (1991).
166. T.G. Muir and E.L. Carstensen. Ultrasound Med. Biol. **6**, 345 (1980).
167. E.L. Carstensen, W.K. Law, N.D. McKay, and T.G. Muir. Ultrasound Med. Biol. **6**, 359 (1980).
168. H.C. Starritt, F.A. Duck, A.J. Hawkins, and V.F. Humphrey. Phys. Med. Biol. **31**, 1401 (1986).
169. G. Du and M.A. Breazeale. J. Acoust. Soc. Am. **80**, 212 (1986).
170. G. Du and M.A. Breazeale. J. Acoust. Soc. Am. **81**, 51 (1987).
171. V. Uhlendorf and F.D. Scholle. *In* Acoustic imaging. Vol. 22. *Edited by* P. Tortoli and L. Masotti, Plenum Press, New York. 1996. p. 233.
172. N. Ichida, T. Sato, and M. Linzer. Ultrasonic Imaging, **5**, 295 (1983).
173. N. Ichida, T. Sato, H. Miwa, and K. Murakami. IEEE Trans. Sonics Ultrasonics, **31**, 635 (1984).
174. T. Sato, A. Fukusima, N. Ichida, H. Ishikawa, H. Miwa, Y. Igarashi, T. Shimura, and K. Murakami. Ultrasonic Imaging, **7**, 49 (1985).
175. C.A. Cain. J. Acoust. Soc. Am. **80**, 28 (1986).
176. T. Sato, E. Mori, K. Endo, Y. Yamakoshi, and M. Sase. Acoustic imaging. Vol. 19. *Edited by* H. Ermert and H.P. Harjes. Plenum Press, New York. 1992. p. 363.
177. Y. Nakagawa, M. Nakagawa, M. Yoneyama, and M. Kikuchi. *In* Proc. 1984 IEEE Ultrasonics Symposium. 1984. p. 673.
178. M.R.T. Tan, H.L. Ransom, Jr., C.C. Cutler, and M. Chodorow. J. Appl. Phys. **57**, 4931 (1985).
179. A. Briggs. Acoustic microscopy. Clarendon Press, Oxford. 1992.
180. F.M. Severin, B. O'Neil, and R.G. Maev. *In* Abstracts review of progress in quantitative nondestructive evaluation. Montreal, Canada. 1999. p. 230.
181. R.G. Maev, D.F. Watt, R. Pan, V.M. Levin, and K.I. Maslov. *In* Acoustic imaging. Vol. 22. *Edited by* P. Tortoli and L. Masotti. Plenum Press, New York. 1995. p. 779.
182. R.G. Maev, V.M. Levin, R.M. Pilliar, E.Yu. Maeva, and T.A. Senjushkina. *In* Acoustic imaging. Vol. 22. *Edited by* P. Tortoli and L. Masotti. Plenum Press, New York. 1995. p. 323.
183. V.M. Levin, R.G. Maev, K.I. Maslov, T.A. Senjushkina, I.G. Grigorieva, and I. Baranchikova. *In* Acoustic imaging. Vol. 19. *Edited by* H. Ermert and H.P. Harjes. Plenum Press, New York. 1991. p. 651.